

# Learning-based 3D Reconstruction in Autonomous Driving: A Comprehensive Survey

Liewen Liao, Weihao Yan, Wang Xu, Ming Yang *Member, IEEE*, Songan Zhang\*

**Abstract**—Learning-based 3D reconstruction has emerged as a transformative technique in autonomous driving, enabling precise modeling of environments through advanced neural representations. It has inspired pioneering solutions for vital tasks in autonomous driving, such as dense mapping and closed-loop simulation. Given the rapid growth in related research, this survey provides a comprehensive review of both technical evolutions and practical applications in autonomous driving. We begin with an introduction to the preliminaries of learning-based 3D reconstruction to provide a solid technical background foundation, then progress to a rigorous, multi-dimensional examination of cutting-edge methodologies, systematically organized according to the distinctive technical requirements and fundamental challenges of autonomous driving. Through an analysis of development trends, we ultimately delineate the challenges and potential directions to inspire future research.

**Index Terms**—Autonomous Driving, Learning-based 3D Reconstruction, Simulation

## I. INTRODUCTION

**A**UTONOMOUS driving has garnered tremendous research attention due to its potential to improve transportation safety and efficiency. Achieving reliable self-driving capability fundamentally hinges on precise perception and a holistic understanding of the 3D environment, which in turn demands large-scale, diverse data collected with a professional sensor suite. However, acquiring such extensive multimodal datasets is expensive and poses safety risks, especially for rare and emergency scenarios. Learning-based 3D reconstruction offers a groundbreaking solution to this challenge. By creating photorealistic and geometrically accurate digital twins of the physical world, 3D reconstruction can synthetically generate abundant training data at a low cost and minimal risk. These virtual yet realistic replicas of driving scenes enable data augmentation and scenario simulation, alleviating the data bottleneck in autonomous driving development.

Over the past few years, the field has witnessed a paradigm shift from traditional techniques to learning-based approaches. Traditional methods have well-known limitations of photogrammetric methods (e.g., structure-from-motion and multi-view stereo) struggle under varying lighting and suffer from distortion, while active sensors (LiDAR, depth cameras) provide accuracy at high equipment and processing cost. The advent of Neural Radiance Fields (NeRF) [1] in 2020 marked

a turning point, demonstrating that neural scene representations can achieve unprecedented fidelity and scalability in 3D reconstruction. NeRF introduced a learning-based modeling approach using neural networks to represent scenes, which significantly outperformed hand-crafted models and prior reconstruction pipelines in rendering novel views with high realism. Building on this foundation, a wave of neural 3D reconstruction techniques [2]–[7] have emerged. In particular, 3D Gaussian Splatting (3DGS) [8] has recently gained prominence as an explicit alternative, representing scenes as sets of 3D Gaussian primitives that can be optimized and rendered directly. This explicit representation yields substantial speed advantages as 3DGS can leverage efficient rasterization with GPU acceleration to achieve real-time rendering, addressing one of NeRF’s key limitations. Together with other advanced neural techniques, NeRF and 3DGS exemplify the rise of learning-based 3D reconstruction methods that overcome many limitations of traditional approaches while offering improved fidelity and efficiency.

Learning-based 3D reconstruction has quickly become a foundational technology in the autonomous driving stack, with far-reaching applications across core tasks. Initially, 3D reconstruction was explored primarily for data augmentation and multimodal sensor simulation [9], [10], but recent research has expanded its role to perception enhancement, improved scene semantics, and end-to-end world modeling for autonomous driving [11]. High-fidelity 3D environment models enrich perception, providing geometric context that can improve object detection and occupancy prediction [12], [13]. Besides, learned 3D models contribute to general scene understanding, as they inherently capture the spatial layout and can be imbued with semantic information [14], [15]. Perhaps most prominently, realistic 3D reconstructions enable immersive simulation by generating virtual cities and scenarios, one can safely test and train autonomous driving systems in a controlled setting [16]–[21]. These reconstructions are increasingly integrated throughout the autonomous driving pipeline, from perception to prediction and planning, underscoring their importance. The rapid proliferation of publications in this area attests to its emerging significance.

Given the transformative developments outlined above, a comprehensive survey of learning-based 3D reconstruction in autonomous driving is timely and valuable. On one hand, the state of the art has advanced rapidly with the introduction of NeRF, 3DGS, and numerous follow-up works, resulting in a flourishing and complex landscape of methods. The volume of related research has grown exponentially in recent years, making it difficult for beginners to obtain a holistic perspective. On the other hand, existing review efforts have

Liewen Liao, Songan Zhang are with the Global Institute of Future Technology, Shanghai Jiao Tong University, Shanghai, 200240, China.

Weihao Yan, Wang Xu, Ming Yang are with the Department of Automation, Shanghai Jiao Tong University, Shanghai, 200240, China

This work was supported in part by the National Nature Science Foundation of China under Grant 52402504 and Grant 62473250. *Corresponding author:* Songan Zhang, email: songanzhang@sjtu.edu.cn.

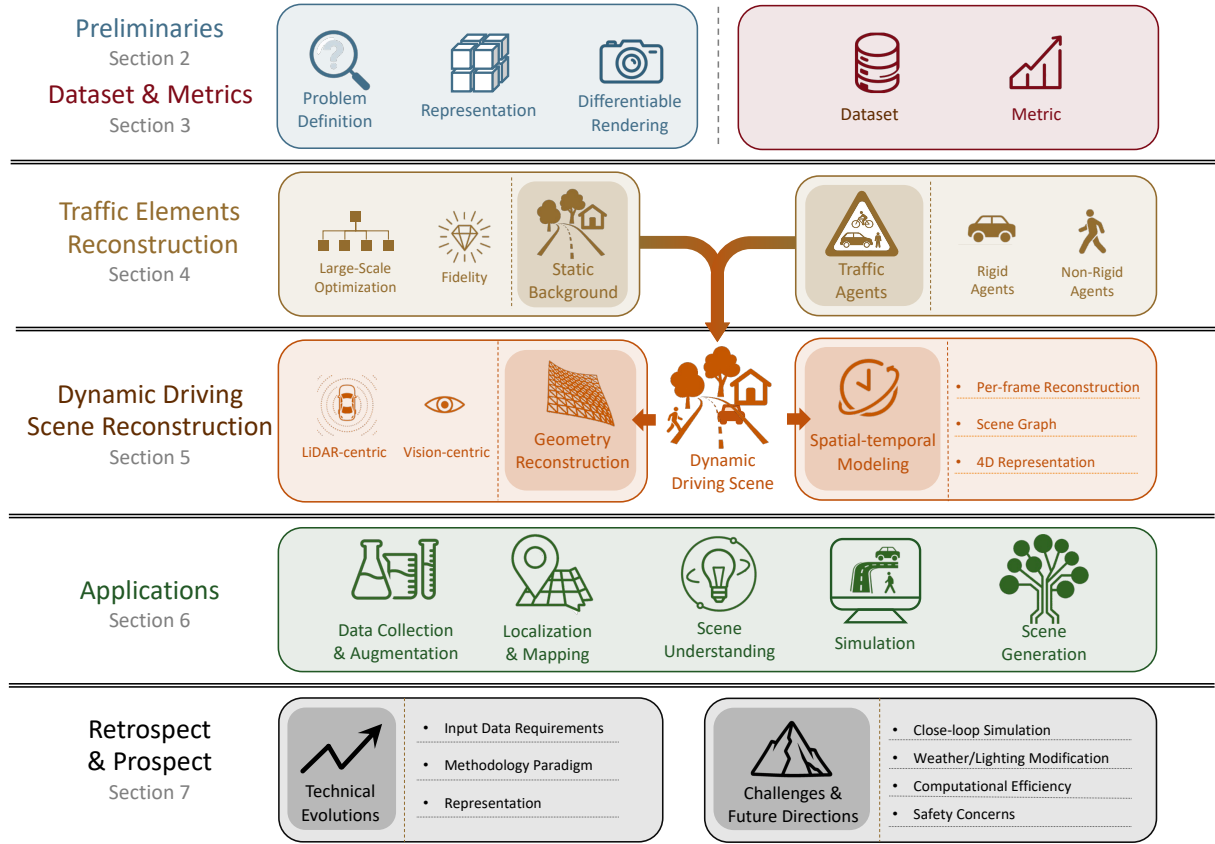


Fig. 1: Survey outlines. We start from preliminaries and essentials of 3D reconstruction, then elaborate on the technical evolutions of traffic elements and dynamic driving scene reconstruction with tailored taxonomy, and diverse applications within autonomous driving. Finally we summarize and delineate challenges and future directions.

been limited in scope. A few recent surveys focus exclusively on specific techniques, such as neural radiance fields [22] or 3D Gaussian splatting [23], [24], or they examine 3D reconstruction outside the autonomous driving context. These surveys provide depth on particular approaches but tend to overlook the broader picture and the cross-technique synergies that are crucial for practical applications within autonomous driving. In contrast, our survey aims to offer a holistic view of the field, bridging multiple methodologies and linking them to practical autonomous driving needs, thereby equipping researchers and practitioners with an authoritative guide to the current state-of-the-art. The contributions of this survey can be summarized as follows:

- **Technical foundation:** We introduce problem definitions, sensor modalities, datasets, and key representation/rendering techniques.
- **Systematic review:** We organize state-of-the-art methods with hierarchical taxonomy based on the practical challenge within autonomous driving.
- **Application-centric view:** We discuss how reconstruction supports core tasks including mapping, simulation, localization, and perception.
- **Future outlook:** We delineate the technical trends and further identify persistent challenges such as simulation

realism, mobile-platform implementation and safety concerns, suggesting future directions.

The organization of this survey is shown in Fig. 1: In Section II, we introduce preliminaries for 3D reconstruction, including problem definition, representation, and rendering methods for learning-based 3D reconstruction. Section III presents the datasets and metrics used to evaluate 3D reconstruction methods. In Section IV, we elaborate on the distinct characteristics and challenges within different elements of the driving scene. Section V systematically examines reconstructions of the dynamic driving scene. In Section VI, we review applications of 3D reconstruction-based technology. Finally, we highlight persisting challenges, safety concerns, and potential directions based on the analysis of development trends in Section VII.

## II. PRELIMINARY

Learning-based 3D reconstruction aims to recover the complete appearance and geometric details with a parameterized model and differentiable optimization. In this section, we will introduce the technical preliminaries of learning-based 3D reconstruction by covering problem definition, representation, and differentiable rendering methods.

### A. Problem Definition

Given a set of observations  $\{o_i, i \in [1, \dots, N]\}$  from perspectives  $\{p_i, i \in [1, \dots, N]\}$ , learning-based 3D reconstruction methods optimize a parameterized scene representation  $F_\theta(\cdot)$  to accurately capture the geometry and appearance, which is commonly formulated as correctly reconstruct observation  $\{\hat{o}_i, i \in [1, \dots, N]\}$  from input views and synthesis observation  $\hat{o}_i, i \in [N+1, \dots]$  from test perspectives  $\{p_i, i \in [N+1, \dots]\}$ . The optimization can be formulated as:

$$\arg \min_{\theta} \sum_i \mathcal{L}(F_\theta(p_i), \hat{o}_i), i \in [1, \dots, N, N+1, \dots] \quad (1)$$

where  $\mathcal{L}(\cdot)$  indicates the reconstruction loss from perspective  $\hat{o}_i$ ,  $F_\theta$  indicates the parameterized representation. With the support of differentiable rendering techniques, this optimization problem can be solved in a gradient-based manner.

### B. Representation

Representation has a profound impact on reconstruction fidelity and computational efficiency, and can be classified into two main categories: implicit and explicit representations. By examining each representation in detail, we aim to highlight their respective advantages and disadvantages. Figure 2 exhibits schematic illustrations of different representations.

#### 1) Implicit Representation:

**Implicit Surfaces** describe the surface of objects with equations, such as Bézier surfaces [25]–[27], Non-Uniform Rational B-Splines (NURBS) [28], [29]. Implicit surfaces provide infinite resolution at arbitrary positions, making them highly suitable for scenarios that require extremely high precision. However, implicit surfaces suffer from prohibitive complexity [25] as the geometry details grow, which hinders the application in practical scenarios.

**Signed Distance Field (SDF)** defines a function that maps a target location to its minimum distance to the surface of the object. SDF utilizes a continuous scalar function to compactly encode geometry by assigning the shortest distance to the surface at each point-positive outside, negative inside, and zero directly on the boundary. SDF provides an efficient option for applications concentrating on geometric while neglecting texture, such as collision calculation [30]–[32] or geometry regularization of other representations [33]–[35].

**Neural Radiance Field (NeRF)** [1] maps target position and viewing direction to the volume density and radiance of the target point. NeRF pioneers optimizing neural representations to synthesize photorealistic novel views in a differentiable manner. However, NeRF suffers from aliasing artifacts and large inference latency arising from the substantial computational overhead in volumetric sampling. These limitations critically hinder real-time rendering, yet drive intensive researches [2]–[4], [36].

#### 2) Explicit Representation:

**Point Cloud** is an unordered set of 3D points that samples the surface of an object or scene. Each point consists of coordinates and additional attributes such as color, intensity [38], or normal vectors compared with the concept in data modality. Its unstructured nature offers flexibility for aggregation and

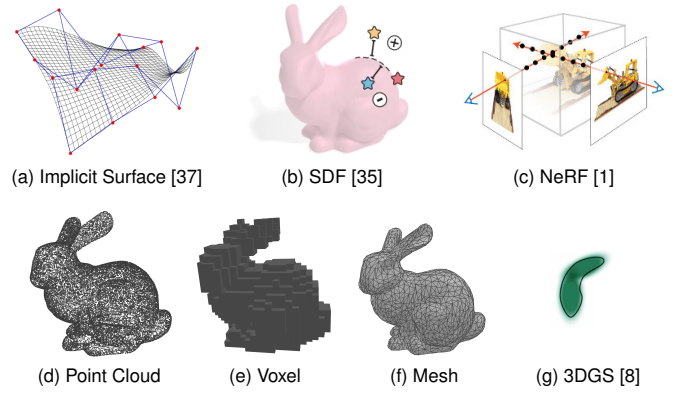


Fig. 2: illustrations of different representations. *Top*: Implicit Representations; *Bottom*: Explicit Representations.

partitioning, but also incurs computational challenges due to the lack of explicit topology.

**Voxel** consists of grid-aligned 3D cubic units that store attributes such as density or color, forming a structured volumetric representation. They capture both surface and internal information, making them well-suited for biomedical and spatial reasoning tasks. Voxel grids allow flexible attribute encoding, from occupancy probabilities and semantic labels [39]–[43] to learnable features in neural networks [44], [45].

**Mesh** is a structured 3D surface representation composed of vertices, edges, and faces, typically 2D triangles or quadrilaterals, connected in a graph-like topology. This structured connectivity enables efficient projection and high-fidelity rendering, making meshes widely used in graphics and engineering. However, their interdependent components increase the complexity of construction and modification.

**3D Gaussians** [8] represent a scene using a set of learnable anisotropic Gaussian ellipsoids, each parameterized by position, covariance (defining shape and orientation), and appearance attributes such as color and opacity. Leveraging the projection-friendly properties of Gaussian functions, 3D Gaussian achieves high rendering fidelity with low computational overhead, making it significantly more efficient than traditional surface- or volume-based methods. While it trades off some GPU memory to support large numbers of Gaussians, this enables real-time, high-quality rendering [46]–[48] and broad applicability, establishing 3D Gaussians as a state-of-the-art representation for both research and practical deployment.

### C. Differentiable Rendering

Unlike traditional rendering, which only simulates image formation, differentiable rendering enables gradient-based optimization of 3D representations by computing the derivatives of reconstruction loss with respect to representation parameters. This approach bridges image supervision and learnable representations in a differentiable pipeline, accelerating convergence and reducing reliance on ground-truth 3D data.

The choice of rendering method has a critical impact on both reconstruction quality and efficiency. Implicit representations typically rely on volume rendering due to projection constraints, while explicit representations support more flexible strategies, with rasterization favored for its efficiency. In

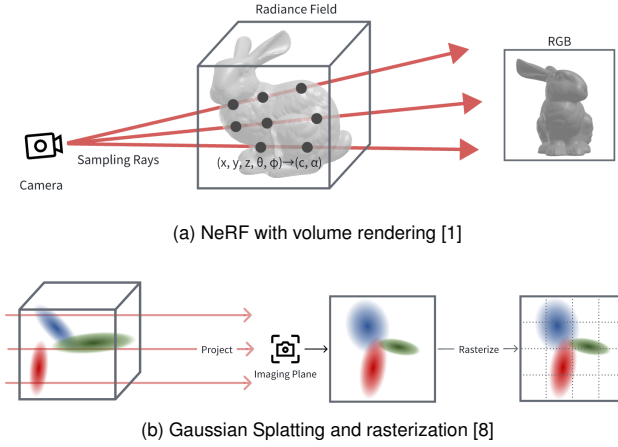


Fig. 3: Rendering Pipeline of NeRF [1] and 3D Gaussian Splatting [8]

the following, we introduce two predominant differentiable rendering approaches as illustrated in Figure 3.

**Volume Rendering** imitates camera to sample the volume through ray-tracing actively. Rays cast from the viewpoint traverse the volume, where each ray represents a pixel, sampling points at discrete positions with parameterized color and opacity. Pixel color is obtained by alpha-blending all sampling points along the ray through opacity-weighted accumulation. Volumetric rendering achieves photorealistic results through physically grounded simulation of light transport, while maintaining compatibility with diverse camera models via parameterized projection matrices. The dual challenges of suboptimal sampling efficiency and the computational complexity of physically accurate material simulations impose a substantial computational cost that hinders real-time rendering.

**Rasterization** projects 3D geometric primitives into discrete pixel-level elements for 2D display. The pipeline projects 3D spatial representations onto the imaging plane, followed by pixel-aligned discretization. Rasterization enables real-time rendering with specific primitives, such as meshes or 3D Gaussians, making it suitable for latency-sensitive tasks. However, the simplified lighting models in rasterization restrict its capacity to model light transport, demonstrating compensated rendering fidelity for advanced materials such as specular surfaces and translucent materials.

### III. DATASETS & METRICS

#### A. Datasets

To reconstruct 3D driving scenes, datasets are essential as they provide synchronized, multimodal inputs paired with rich annotations, such as 3D bounding boxes, semantic labels and HD map. These datasets can be broadly categorized into full-scene collections that capture diverse driving scenarios and object-centric collections that offer detailed modeling of individual traffic participants. Together, both types establish the foundational training and evaluation benchmark for holistic scene understanding and precise object reconstruction in autonomous driving.

1) *Object-centric Dataset*: Object-centric datasets provide support for high-precision reconstruction of specific traffic participants. Based on the objects within the datasets, they can be categorized into vehicle datasets and human datasets.

**Vehicle datasets** provide multi-view observations of vehicles, offering essential priors for sparse-view reconstruction of vehicles. Multi-view Marketplace Car (MVMC) [49] contains approximately 6,000 images of 600 vehicle models, while CarPatch [50] collects 530,101 images of varying quality from the internet. PandaCar [51] and 3DRealCar [52] further include LiDAR point clouds, providing precise geometric information. Additionally, 3DRealCar [52] provides detailed vehicle component segmentation masks, laying a data foundation for future component-level reconstruction.

**Human Datasets** To date, a dedicated pedestrian-specific 3D reconstruction dataset remains absent, and existing research relies on human digitization datasets. Series such as Human3.6M [53], Fit3D [54], CHI3D [55], FlickrSC3D [56], HumanSC3D [56], and 3DPW [57] provide indoor-captured human motion data, enabling posture reconstruction, but their predefined synthetic human geometry and lack of appearance details fail to meet 3D reconstruction requirements. RenderPeople [58] offers high-quality, paid 3D human models with diverse genders, ethnicities, and clothing, some of which include motion and facial expressions, providing rich and detailed human data. However, real-world pedestrian characteristics differ significantly from these datasets, primarily due to severe occlusions, diverse behavioral patterns, and varying outdoor lighting conditions. All these differences jointly pose substantial challenges for pedestrian data collection.

2) *Full-scene collections*: Full-scene collections are particularly valuable for autonomous driving as they capture the complete spatial and temporal context of driving environments, enabling models to understand complex inter-object relationships, scene dynamics, and the holistic geometric structure necessary for comprehensive autonomous driving perception. Full-scene collections can be categorized into multimodal datasets obtained by professional sensor suites, and unimodal datasets collected from public sources. Detailed comparison among full-scene data collections is shown in Table I.

Multimodal datasets provide rich sensor data, including images, calibration, and LiDAR point clouds, along with comprehensive annotations such as 2D/3D bounding boxes, semantic segmentation, and HD maps. Commonly used multimodal datasets include the KITTI series [59], [62], [65], [67], [69], Cityscapes [60], NuScenes [63], Waymo Open Dataset [64], and Argoverse [66], [70]. Table I provides a horizontal comparison of datasets across several key aspects, including data modalities, annotations, resolution, and diversity to highlight their distinct advantages. KITTI [59], as the first driving scenario dataset, has been widely applied but is limited by lower data resolution and diversity, leading to the development of several derivative or iterative datasets. NuScenes [63] and Argoverse2 [66] offer surround-view perspectives, providing the most comprehensive image observations. Waymo [64] delivers high-quality LiDAR point clouds utilizing two high-precision LiDARs with an expanded field of view compared with NuScenes. NOTR [68] is a subset



TABLE I: Overall comparison between full-scene data collections.

Dataset	Year	Type	Modality			Annotation		Volume		Resolution	Frame Rate		Sem. Types	Weather Types	Time of Day	Scenario Types
			Image	Depth	PCL	BBox	Semantic	Scenes	Image		Camera	LiDAR				
KITTI [59]	2012	Real	✓	✓	✓	3D	-	22	15K	1242×376	10	10	8	1	1	2
CityScapes [60]	2016	Real	✓	✓	-	-	✓	50	25K	2048×1024	-	-	30	2	11	3
BDD100K [61]	2018	Real	✓	-	-	2D	✓	100k	12M	1280×720	30	-	40	5	2	4
SemanticKITTI [62]	2019	Real	-	-	✓	-	✓	22	43552	-	-	10	28	1	1	4
NuScenes [63]	2019	Real	✓	-	✓	3D	✓	1000	1.4M	2048×1536	12	10	23	3	2	4
Waymo [64]	2019	Real	✓	-	✓	3D	✓	1150	390K	1920×1080	10	10	23	2	3	5
VirtualKITTI2 [65]	2020	Syn.	✓	✓	-	3D	✓	5	20992	1242×375	#	-	8	3	2	5
Argoverse2 [66]	2021	Real	✓	-	✓	3D	✓	1000	6M	2048×1550	20	10	30	2	1	1
KITTI-360 [67]	2022	Real	✓	-	✓	3D	✓	11	150K	1408×376	#	#	37	1	1	1
NOTR [68]	2023	Real	✓	-	✓	3D	✓	120	#	1920×1080	10	10	23	#	#	#

**All Column:** “-” —Absence of corresponding modality; “#” —Not mentioned.

**Type:** “Real” —Collected in real world; “#” —Synthesized.

**Annotation-BBox:** 3D—3D Bouding Box; 2D—2D Bounding Box

selected from the Waymo Open Dataset containing 120 challenging driving scenes, enriched with additional annotations including 2D bounding boxes for dynamic objects, ground truth 3D scene flow, and 3D semantic occupancy. Unimodal datasets, primarily represented by BDD100K [61], collect an unparalleled scale of driving scenario videos from the internet but are constrained by simple GPS location information and variable video quality.

## B. Metrics

1) *Pixel-wise Metric*: Pixel-wise metrics evaluate reconstruction quality by directly comparing pixel values between generated and reference images using measures like Mean Squared Error (MSE), Mean Absolute Error (MAE), and Mean Absolute Percentage Error (MAPE). While computationally efficient, these metrics often fail to capture perceptual quality.

2) *Perceptual Metric*: Perceptual metrics evaluate reconstruction quality by modeling human visual perception rather than direct pixel comparisons. These metrics assess structural and textural similarity, including edge preservation and overall visual coherence. Typical perceptual metrics include Structural Similarity Index Measure (SSIM) for structural assessment, as well as feature-based metrics like Learned Perceptual Image Patch Similarity (LPIPS) [71] and VGG loss [72], which operate in learned representation spaces. While these metrics correlate better with human quality judgments, they require greater computational resources than pixel-wise alternatives.

3) *Generative Metric*: Generative metrics evaluate the quality of synthetic content by assessing how closely generated data distributions align with real-world distributions. Key metrics include Inception Score (IS) [73] for evaluating image quality and diversity, Fréchet Inception Distance (FID) [74] for comparing feature distributions between generated and authentic images, Fréchet Video Distance (FVD) [75] for temporal content evaluation, and Maximum Mean Discrepancy (MMD) [76] for quantifying distribution divergence. These metrics specifically measure the statistical alignment between generated and reference data distributions.

## IV. TRAFFIC ELEMENTS RECONSTRUCTION

The driving scenario comprises diverse complex elements that can be functionally categorized into static backgrounds

and traffic agents. The static background establishes the environmental foundation of the driving scene, while traffic agents serve as primary interactive objects during driving. Their distinct characteristics pose different challenges for 3D reconstruction.

### A. Static Background Reconstruction

Static background elements, including roads, buildings, vegetation, and traffic infrastructure, constitute the environmental foundation for autonomous driving systems. Reconstructing these elements presents dual challenges: achieving high fidelity reconstruction while managing the computational complexity of large-scale optimization. This section analyzes existing methods addressing these challenges and examines their practical applications in autonomous driving. Table II exhibits detailed information and performance of static background reconstruction methods.

1) *Fidelity*: High-fidelity static background reconstruction is fundamentally crucial to alleviate the sim-to-real gap in autonomous driving systems. It can provide a stable and accurate reference for downstream tasks that require precise capture of both spatial geometry and visual appearance of the driving environment. Reconstruction quality fundamentally depends on the choice of 3D representation, with different representations offering unique strengths and weaknesses.

**Geometry Fidelity** Novel learning-based representations, NeRF and 3D Gaussians, demonstrate significant advantages in visual quality through differentiable rendering, yet geometric fidelity of these representation remains unsatisfactory.

NeRF [1] enables photorealistic rendering, but the lack of explicit geometric constraints results in limited geometric fidelity. PlaNeRF [78] introduces an SVD-based regularization term to enhance the geometric quality of road surfaces while StreetSurf [77] integrates SDF as geometry regularization. AlignMiF [79] advances deep multimodal alignment research by systematically investigating LiDAR-camera misalignment issues when incorporating LiDAR data. AlignMiF proposes a geometry-aware alignment module to enhance geometry fidelity by utilizing a LiDAR prior.

3DGS struggles to maintain precise geometric reconstruction due to the fixed ellipsoidal shape of Gaussians, particularly for flat surfaces like roads or walls. [84], [85], [87], [88] leverage distinct geometric priors of different scene elements,

TABLE II: Comparison among static background reconstruction methods.

Scene Repr.	Method	Input			Occl. Idn.	Par. Cri.	Output						Training		FPS	Dataset					Open Source
		Image	Calibration	Point Cloud			Image	Depth	Normal	Point Cloud	Semantic	Mesh	Devices	Hours		Waymo	KITTI	NuScenes	KITTI-360	Others	
NeRF	StreetSurf [77]	✓	✓	A		Dist.	✓	✓	✓	✓	✓	✓	1×RTX3090	1.5		26.66	✓	✓			✓
	PlaNeRF [78]	✓	✓	-	Sem.		✓	✓		✓	✓	✓	1×RTX3090	2.5							
	AlignMiF [79]	✓	✓	I	Sem.		✓	✓		✓			1×RTX3090	2.5		29.78			✓	[80]	✓
PCL	Neural Point Light Field [81]	✓	✓	I			✓	✓		✓			1×V100	48		31.25	✓	✓			✓
	DGMR [38]	✓	✓	-		Spa.	✓			✓			1×V100		16.67		✓	✓		[60] [70]	
Mesh	DNMP [82]		✓	I			✓	✓		✓	✓	✓	1×A100			27.62			✓		✓
	RoMe [83]	✓	✓	-	Sem.	Smpl.	✓	✓		✓	✓	✓	1×RTX3090	2			✓	✓			✓
	EMIE-MAP [14]	✓	✓	S			✓				✓	✓	1×A100				✓				
3DGS	DHGS [84]	✓	✓	I	Sem.	Dist.	✓	✓								28.09					
	StreetSurfGS [85]	✓	✓	I		Tem.	✓	✓	✓			✓	1×RTX3090			28.67			✓		
	HGS-Mapping [87]	✓	✓	I			✓	✓	✓	✓		✓	1×RTX3090			26.45	✓	✓		[86] [65]	
	GVKF [88]	✓	✓	I			✓	✓	✓			✓		1.5	32	30.24					✓
	StreetUnveiler [89]	✓	✓	I	Sem.		✓	✓	✓			✓								[90]	✓

**Input-Point Cloud:** A—Optional Augmentation; S—Supervision; I—Input.

**Occl. Idn.:** Occlusion identification. **Sem.**—Semantic Segmentation; **Uncer.**—Uncertainty.

**Par. Cri.:** Spa.—Spatial; Dist.—Distance to Ego; Smpl.—Waypoint Sampling; Tem.—Temporal Chunk.

**Dataset:** Num.—PSNR of reconstruction; ✓—Evaluated on.

**Open Source:** ✓—released to the public; ★—Recognized Method; U—Unofficial implementation.

enabling the design of tailored Gaussian variants that enhance the quality of geometry and appearance reconstruction, such as spherical Gaussians for sky modeling [87], planar 2D Gaussians for road surface [87], [91]. To alleviate the distortion brought by discrete Gaussian primitives, DHGS [84] further incorporates an SDF as auxiliary implicit surface representation to regularize the near-road reconstruction. Gaussian Voxel Kernel Function (GVKF) [88] combines 3D Gaussian with continuous surface modeling capability of implicit representation, providing a hybrid representation that offers a novel alternative for geometry-sensitive downstream applications.

**Photorealism** Traditional explicit representations, including point clouds and meshes, demonstrate impressive geometric flexibility in reconstruction, enabling accurate modeling of arbitrary geometry. However, their limited representation capacity fails to encode fine-grained visual details within a tolerable cost. Approaches integrate differentiable neural representations with explicit representations to achieve photorealistic rendering.

Neural point light field [81] encodes the local light field into each point as neural features, enhancing the spatial capacity of each point. Combined with differentiable volumetric rendering for optimization, it achieves high-quality rendering results. DGMR [38] extracts feature points from the density field of NeRF, employing depth regularization to eliminate outliers and enhance geometric quality. Additionally, it designs a UNet architecture to decode the feature points into images, achieving improved reconstruction of both geometry and appearance.

RoMe [83] and EMIE-MAP [14] propose specialized neural mesh representations for road surface reconstruction. RoMe [83] assigns each vertex fixed 2D coordinates, learnable elevation, RGB, and semantic features. However, direct optimization of RGB leads to convergence instability due to varying observation direction and lighting conditions. EMIE-MAP [14] builds on RoMe by replacing direct RGB values with implicit RGB features, stabilizing the training process and improving reconstruction quality. In contrast, DNMP [82]

enables more flexible reconstruction by learning both the position and appearance of vertices for diverse static components like roads, vegetation, and buildings.

2) *Large-scale Optimization:* The static background in autonomous driving scenarios typically manifests as unbounded, long-range environments encompassing multi-scale elements with diverse material properties, creating significant challenges for high-quality reconstruction while maintaining computational efficiency. To address these large-scale optimization challenges, researchers have adopted scene decoupling strategies that can be categorized into two primary approaches based on their underlying principles.

Content-agnostic methods partition scenes using uniform criteria such as spatial location [38], temporal data slices [85], or data sampling points [83]. These approaches divide environments into regular partitions and apply consistent spatial representations across all segments.

Conversely, content-aware methods leverage scene-specific characteristics by decoupling based on distance to the camera [77] or element types [84], such as distinguishing road surfaces from non-road elements. This decoupling method enables customized representations tailored to each segment's unique properties. For instance, StreetSurf [77] employs distance-based segmentation to create components with varying detail levels, allowing for optimal NeRF variants for each segment, while DHGS [84] separates road surfaces from other elements, proposing specialized planar 2D Gaussians regularized by SDF for nearby road surfaces.

## B. Traffic Agents Reconstruction

While static background reconstruction establishes the environmental foundation, traffic agents, encompassing vehicles, cyclists, and pedestrians, represent the core interactive elements that autonomous driving systems must accurately perceive and understand. High-quality reconstruction of these dynamic participants is critical for enabling essential capabilities such as object detection and tracking, behavior prediction, and

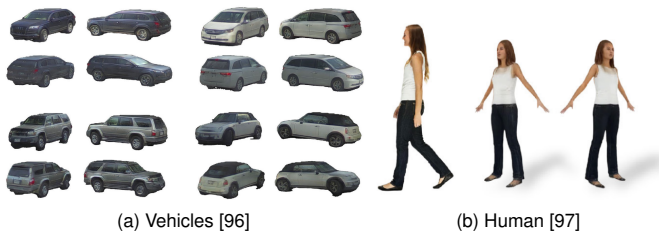


Fig. 4: 3D reconstruction of traffic agents.

collision avoidance. Traffic agents can be naturally categorized based on their deformation properties, which fundamentally determines the reconstruction approach required: rigid agents maintain a fixed shape during motion, allowing them to be reconstructed as a static object within their local coordinate, while non-rigid agents, including cyclists and pedestrians, exhibit complex articulated movements and shape variations that demand specialized deformation modeling techniques.

1) *Rigid Agents Reconstruction*: Rigid agents are characterized by non-deformable and symmetric properties, which facilitate their reconstruction.

Vehicles are typically modeled as rigid agents. Due to the significant color variations within the same model, independently modeling the geometry and appearance of vehicle is an practical approach. CADSim [92] introduces predefined CAD models as geometry initialization priors to enhance fidelity and accelerate convergence, subsequently fine-tuning geometry and appearance through differentiable rendering. Car-Studio [50] incorporates separate shape and texture components with mip-NeRF architecture while NeuSim [51] leverages point cloud to construct a preliminary geometry using an SDF, then models RGB and shading features with NeRF. DreamCar employs a hierarchical NeRF framework comprising three specialized models [1], [93], [94] to achieve coarse-to-fine geometry reconstruction and incorporates generative models to provide high-resolution textures.

Mirror symmetry is a key characteristic of vehicles, effectively mitigating the reconstruction challenges posed by sparse observations. NeuSim [51] applies mirror symmetry when constructing the geometric SDF from point clouds to complete the occluded side, and DreamCar [95] employs mirror flipping during data processing to augment the dataset.

Despite the reconstruction methods, GenAssets [96] proposed a unified 3D asset generation framework applicable to diverse agents, including pedestrians and cyclists, by treating them as rigid agents (Fig 4). GenAssets encodes diverse agents into a low-dimensional latent distribution, thereby enabling high-quality 3D asset generation through a diffusion model.

2) *Non-rigid Agents Reconstruction*: Pedestrians and cyclists present significant reconstruction challenges due to their complex articulated movements and continuous shape variations during motion. Linear Blend Skinning (LBS) serves as a popular technique for 3D human body reconstruction, which first reconstructs the body in canonical space and parameterizes body deformations as skeletal pose variations, enabling reconstruction under arbitrary poses. Early LBS-based approaches [132]–[134] integrate pose estimation with

spatial representations such as occupancy grids or meshes, enabling dynamic reconstruction of human geometry and motion from video sequences. However, these methods fail to recover visual details due to the inherent complexity of modeling both deformation and photometric properties simultaneously. Recent advances in human body reconstruction [97], [135]–[140] have introduced novel spatial representations into the LBS framework, achieving dual improvements in both photorealism and geometric fidelity. Notably, 3DGS-based methods [97], [138]–[140] further enable real-time rendering capabilities within this enhanced framework. However, these methods have only been validated on close-range, high-quality human digitization datasets, necessitating further research to address the challenges of distant, heavily occluded pedestrians in outdoor driving scenarios.

## V. DYNAMIC DRIVING SCENE RECONSTRUCTION

Beyond individual element reconstruction, dynamic driving scene reconstruction faces several fundamental challenges caused by agent motion, including reconstructing high fidelity geometry with minimal observation overlap, developing effective spatial-temporal modeling strategies to represent scene dynamics, achieving computational efficiency for real-time deployment, and generating appropriate output modalities to support various autonomous driving tasks. The following analysis examines existing methods across these dimensions, highlighting how different approaches balance reconstruction quality, computational requirements, and task-specific applicability. Table III exhibits detailed information and performance of dynamic scene reconstruction methods.

### A. Geometry Reconstruction

Dynamic driving scenarios captured from the ego-view perspective exhibit minimal cross-view overlap, posing increased difficulty to geometry reconstruction. Based on the different dependency on input data modalities, methods can be categorized into LiDAR-centric methods that leverage point cloud inputs for geometric recovery explicitly and vision-centric methods that estimate geometry solely from image.

1) *LiDAR-centric*: RGB images provide rich visual details but lack geometric information, particularly in dynamic driving scenes with limited multi-view observations. LiDAR point clouds, on the other hand, offer precise geometric information but often exhibit sparse characteristics. LiDAR-centric methods utilize both to achieve complementary advantages.

Point clouds in LiDAR-centric frameworks serve two distinct technical functions: as supervisory signals to guide the optimization process or as initialization priors within direct inputs. As supervisory signals, point clouds generate ground-truth depth maps through imaging-plane projection, which supervise rendered depth maps to optimize either sampled points [9], [68], [77], [102], [104], [107], [108], [124]. Alternatively, other approaches directly leverage the inherent geometric information within point clouds to achieve near-optimal initialization, thereby avoiding sub-optimal solutions and accelerating convergence. Point cloud-based [81], [82], [141] and part of 3DGS-based methods require high-precision

TABLE III: Overall comparison among comprehensive scene reconstruction, generation methods and simulators.

Task	Repre.	Method	Input			Decomp.	Rendering							Devices	FPS	Dataset						Open Source
			Image	Pose	Point Cloud		Image	Depth	Point Cloud	Veh. Pose	Instance	Semantic	Flow			KITTI	Waymo	NuScenes	vKITTI2	KITTI-360	Others	
Recon.	PCL	READ [98]	✓	✓	Input	BBox	✓							RTX2070		23.286					[99]	*
		NSG [100]	✓	✓	-	BBox	✓							RTX6000	0.032	26.66			✓			✓
		PNF [101]	✓	-	-	Self	✓	✓		✓	✓	✓				27.48			✓	✓		
		NeuRAD [102]	✓	✓	SV.	BBox	✓	✓	✓							27.91		✓			[66] [103]	*
		SUDS [9]	✓	-	SV.	Self	✓	✓		✓	✓	✓	S	RTX6000	0.01	28.31			✓			✓
		EmerNeRF [68]	✓	✓	SV.	Self	✓	✓	✓				S	RTX6000	0.053		28.87					*
		ProSGNeRF [104]	✓	✓	SV.	BBox	✓	✓								30.31			✓			*
		DiCo-NeRF [105]	✓	✓	-	Self	✓	✓												✓	[106]	S
	NeRF	S-NeRF [107]	✓	✓	SV.	BBox	✓	✓						RTX6000	0.02		23.60	✓				✓
		S-NeRF++ [108]	✓	✓	SV.	BBox	✓	✓				✓	O				25.78	✓				
		DrivingGaussian [109]	✓	✓	AUG.	BBox	✓											✓		✓		✓
		GGRt [110]	✓	-	-	-	✓	✓								22.59	32.12					✓
		TCLC-GS [111]	✓	✓	Input	-	✓	✓						RTX3090ti	90		28.11	✓				
		SGD [112]	✓	✓	Input	-	✓	✓								23.85*				✓		
		HO-Gaussian [113]	✓	✓	-	-	✓							V100	71		28.03				[66]	
		S <sup>3</sup> Gaussian [114]	✓	✓	Input	Self	✓	✓									32.14				[68]	✓
	3DGS	PVG [115]	✓	✓	Input	Self	✓	✓				✓	V	RTX6000	59	32.83	32.46					✓
		Street Gaussians [116]	✓	-	Input	BBox	✓	✓		✓				RTX4090	135	25.79*	34.61					*
		OmniRe [117]	✓	✓	Input	BBox	✓	✓						RTX4090	60		34.25					*
		DeSiRe-GS [118]	✓	✓	Input	Self	✓	✓					V	RTX4090	36	33.94	33.61					✓
		VDG [119]	✓	-	-	Self	✓	✓						V100	61	31.61	31.65					S
		HUGS [120]	✓	✓	Input	BBox	✓	✓			✓	✓	O	RTX4090	93	28.78			✓	✓		✓
		VEGS [121]	✓	✓	Input	BBox	✓	✓						RTX3090	144	24.77				✓		✓
		AutoSplat [122]	✓	✓	Input	BBox	✓	✓								26.59*					[90]	
	Gen.	GGs [123]	✓	✓	Input	-	✓	✓								29.12					[99]	
		DriveDreamer4D [124]	✓	✓	SV.	BBox	✓	✓														✓
		DrivingForward [125]	✓	-	-	Self	✓	✓														✓
		SplatAD [126]	✓	✓	Input	BBox	✓	✓	✓									✓			[66] [90]	S
		DreamDrive [127]	✓	✓	Input	-	✓	✓										✓				
		STORM [128]	✓	✓	SV.	Self	✓	✓					S				26.38				[66]	*
		EMD [129]	✓	✓	Input	B/S	✓	✓					S				32.5					S
		Omni-Scene [44]	✓	✓	-	-	✓	✓										✓				✓
		Uni-Gaussians [10]	✓	✓	Input	BBox	✓	✓	✓								29.62		✓			
Sim.	3DGS	UniScene [130]	-	-	-	BBox	✓	✓	✓		✓							✓				S
		MagicDrive3D [131]	-	-	-	BBox	✓	✓	✓	✓								✓				S
	NeRF	UniSim [16]	✓	✓	Input	BBox	✓	✓	✓	✓											[90]	*
		MARS [18]	✓	✓	-	BBox	✓	✓						RTX6000	0.03	29.06			✓			✓
		NeuroNCap [19]	✓	✓	-	BBox	✓	✓		✓								✓				✓
		OASim [17]	✓	✓	AUG.	BBox	✓	✓	✓	✓								✓				✓
		ChatSim [21]	✓	✓	Input	BBox	✓	✓	✓	✓							25.82					✓
	G.S.	HUGSIM [20]	✓	✓	-	BBox	✓	✓	✓	✓	✓	✓	O	RTX3090	89	27.40	28.79	✓	✓	✓		*

**Task:** Recon.—Comprehensive Scene Reconstruction; Gen.—Generation; Sim.—Simulator.

**Repre.** Representation: PCL—Point Cloud.

**Input-Point Cloud:** SV.—Supervision; AUG.—Optional Augmentation.

**Decomp.** Decomposition: BBox—3D Bounding Box; Self—Self-supervised; B/S—3D Bounding Boxes or Self-supervised.

**Rendering-Flow:** S—3D Scene Flow; O—2D Optical Flow; V—Velocity Map.

**Dataset:** ✓—Evaluated on; Num.—PSNR of reconstruction in dB; \*—PSNR of Novel View Synthesis.

**Open Source:** ✓—Released to the Public; \*—Recognized Method; S—Officially Announced Coming Soon.

LiDAR point clouds [114]–[118], [121], [122], [126], [129] while others [120], [123], [127] utilize SfM or COLMAP point clouds as an approximate substitute. [112] further utilizes images and LiDAR point clouds as conditions for a video diffusion model to synthesize 3D Gaussians directly.

2) *Vision-centric*: Early vision-centric approaches [100], [105] primarily assessed rendering fidelity while neglecting geometric accuracy, resulting in incomplete 3D scene reconstruction. PNF [101] undergoes pre-training on ShapeNet [142] to acquire vehicle shape priors, which facilitate geometric structure initialization in the model. [110], [113] enhance geometric reconstruction by strengthening epipolar correspondence across consecutive frames. Specifically, HO-Gaussian [113] generates virtual viewpoints with minimal displacements through linear transformations, while GGRt [110] employs cross-attention mechanisms to establish correlations among sampled points along epipolar rays. DrivingForward [125] constrains depth estimation accuracy by enforcing consistency of rendered depth map across multi-perspective surround-view images, thereby enhancing geometric reconstruction quality. VDG [119] employs off-the-shelf visual odometry for monocular depth estimation, subsequently

achieving geometric reconstruction through inverse projection.

Accurate 3D geometry recovery from 2D images necessitates the construction of precise camera models, where the correctness of calibration parameters plays a critical role. However, calibrations obtained during high-speed motion, particularly for extrinsic parameters, are typically noisy and rely on costly manual corrections. This has driven some methods to seek independence from calibration inputs. VDG [119] estimates and refines extrinsics through a pre-trained visual odometry, while DrivingForward [125] uses fixed vehicle-to-camera and inter-frame camera motion to eliminate dependency on camera extrinsics.

### B. Spatial-temporal Modeling

The dynamic behavior of agents introduces complex spatial-temporal relationships that transform driving scenarios from static 3D reconstruction into dynamic 4D modeling challenges. Existing approaches for capturing these spatial-temporal dynamics can be categorized into three primary strategies: per-frame reconstruction methods that independently process temporal snapshots, scene graph-based approaches that simplifies dynamics as object bounding box movements, and native 4D



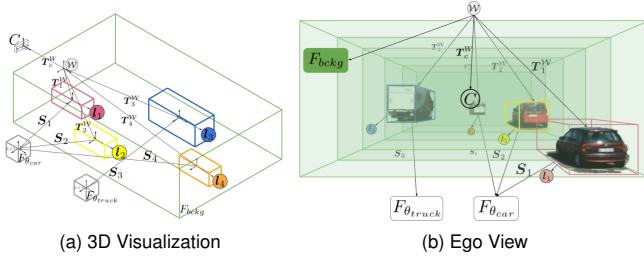


Fig. 5: Decoupling Paradigm of Neural Scene Graph [100]. Agents are modeled in corresponding local coordinates and resembled into complete scene in global coordinates with transformation and scaling (visualized in arrow).

representation methods that uniformly encode time-varying scene properties across the entire spatial-temporal domain.

1) *Per-frame Reconstruction*: Per-frame reconstruction decouples temporal frames and computes an independent 3D representation for each frame, which shrinks the temporal scale to a single or a few frames. This pipeline significantly simplifies the complexity of spatial-temporal relationships, facilitating feedforward methods [44], [125] in straightforward model and loss design. [44], [125] perform per-frame per-pixel Gaussian predictions while [125] enhances spatial-temporal consistency by leveraging multi-view and multi-frame inputs as prediction context. Nonetheless, this pipeline overlooks cross-frame consistency, particularly within static elements, introducing significant redundancy in 3D representations and resulting in unnecessary computational and storage overhead.

2) *Scene Graph*: As a pioneering work in dynamic driving scene reconstruction, NSG [100] proposes Scene Graph to model spatial-temporal relationships by decomposing dynamic driving scenes into individual agents with their associated bounding boxes and radiance properties (Fig 5). This approach simplifies temporal dynamics to object-level transformations of bounding boxes over time, enabling the reconstruction of agents in their own canonical frame, and has been adopted in subsequent methods [10], [98], [102], [104], [107]–[109], [117], [120]–[122], [126]. Beyond reconstruction, Scene Graph enables users to readily achieve parameterized control of agents within the scene with different object arrangements and the creation of novel scene compositions by integrating agent pose control modules, giving rise to a series of open-loop and close-loop simulators [16]–[20].

However, scene graph modeling faces two significant limitations in driving scenarios. First, scene graph methods critically depend on accurate 3D bounding boxes, which impose substantial computational costs whether obtained through manual annotation or automated detection and tracking systems. The inherent noise and inaccuracies in 3D bounding box estimation further degrade scene graph fidelity. To address these challenges, HUGS [120] introduces learnable kinematic parameters combined with unicycle model-based regularization to improve 3D bounding box estimation while reducing reliance on external detection systems. Second, the rigid body assumption inherently fails to capture non-rigid deformations in

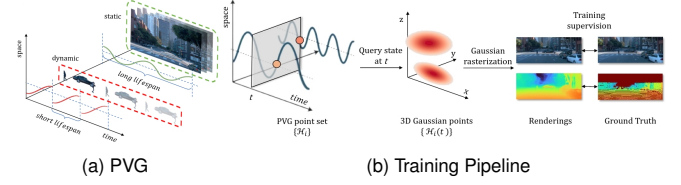


Fig. 6: Illustration of Periodic Vibration Gaussian (PVG) [115]. (a): Static background with long lifespan and dynamic agents with short ones; (b): Pipeline of PVG. Zoom-in for details.

dynamic agents such as pedestrians and cyclists. While some approaches [10], [117] attempt to address this by integrating parametric models like SMPL for human representation, the resulting appearance artifacts limit practical deployment. Despite these advances, research in scene graph-based dynamic reconstruction remains active, with ongoing efforts to further address the limitations mentioned above.

3) *4D Representations*: By elevating static 3D representation into dynamic 4D space via introducing an additional temporal dimension, 4D representations enable native modeling of spatial-temporal relationships for both rigid and non-rigid agents without compromises [9], [68], [105], [114], [115], [118], [119], [124], [127], [128]. NeRF-based methods [9], [68] utilize a separate dynamic component to represent dynamic agents within the scene, which accepts time as an additional input to the radiance field, reformulating the color and density as time-varying attributes. Some Gaussian-based works [124], [127] model 4D Gaussians as a combination of a 3D Gaussian representing the initial state and a time-varying offset of each attribute, forming a basic form of 4D Gaussian. Periodic Vibration Gaussian (PVG) [115] proposes a novel spatial-temporally unified representation based on 3DGS (Fig. 6) for modeling time-varying dynamic elements and is adopted by [118], [119]. PVG reformulates the mean and opacity of traditional 3D Gaussian into continuous time-dependent functions with learnable lifespan, extending 3D Gaussian from reconstruction to analytical primitive.

Beyond natively representing scene dynamics, 4D representation-based methods also eliminate reliance on external bounding box annotations by achieving self-supervised dynamic-static decomposition during reconstruction. These approaches employ various strategies for automatic scene segmentation. DiCoNeRF [105] identifies dynamic objects by computing cosine similarity between ground truth and rendered features, while  $S^3$ Gaussian [114] utilizes spatial-temporal Hexplane features to separate static and dynamic elements, with dynamic agents naturally captured on temporally varying planes. [127] employs a two-stage approach, first constructing a time-invariant static model with 3D Gaussians, then identifying dynamic agents as regions exhibiting large rendering errors. PVG-based methods offer additional flexibility through learnable attributes as PVG [115] dynamically allocates learnable lifespans and velocities to scene elements during training, enabling subsequent works [118], [119] to derive motion masks from

velocity attributes for static-dynamic decoupling explicitly.

4D representation demonstrates notable advantages in processing complex driving scenarios due to its capacity to simultaneously handle both rigid and non-rigid agents without relying on any a priori assumptions or compromises. Furthermore, the self-supervised dynamic-static decomposition based on 4D representation eliminates the dependency on costly 3D bounding box annotations, thereby establishing it as the most promising spatiotemporal paradigm for future applications.

## VI. APPLICATIONS

### A. Data Collection & Augmentation

3D reconstruction provides a scalable and cost-effective solution for data acquisition and augmentation. Contemporary frameworks are increasingly adopting multiple rendering modalities to holistically simulate field-acquired datasets with physically-grounded sensor responses and diverse fine-grained semantic annotations. Figure 7 demonstrates different rendering modalities and annotations in autonomous driving.

**Image** constitutes an indispensable component across all methods as the most fundamental modality in 3D reconstruction. Notably, DiCo-NeRF [105] stands out as one of the few works implementing fisheye-view rendering, providing critical support for panoramic perception systems and solutions.

**Depth Image** is adopted by most methodologies [9], [44], [68], [101], [102], [104], [107], [108], [110]–[112], [114]–[121], [123]–[126], [128] as 2D geometric proxies for spatial information, where 3D scene geometry is projected onto the 2D imaging plane via perspective transformation. Although depth images retain partial spatial cues (e.g., relative distances), they inherently incur lossy spatial encoding due to dimension reduction, discarding critical 3D structural details (e.g., surface normals, multi-view consistency) and introducing ambiguity in occluded regions.

**Point Cloud** has gradually garnered significant attention with the increasing adoption of LiDAR in autonomous driving systems. It can be synthesized with LiDAR simulation in scene reconstruction. Due to the uniqueness of the imaging method, LiDAR point clouds exhibit distinct characteristics compared with 2D images. LiDAR ray drop probability and rolling shutter effects from sequential scanning during rapid vehicle movement are explicitly modeled by [102], [126], enabling more realistic multimodal simulation. EmerNeRF [68] models asynchronous LiDAR sampling via depth and line-of-sight constrained volumetric rendering. SplatAD [126] develops a projection algorithm in spherical coordinates and customizes a tiling, sorting, and rasterization pipeline tailored for imitating the imaging process of LiDAR. Uni-Gaussians [10] combines ray-tracing and rasterization into a high-fidelity, efficient framework for joint camera-LiDAR simulation, using bounding volume hierarchy and custom CUDA kernels to accelerate LiDAR ray-tracing.

**Segmentation** plays a vital role in perception modules. PNF [101] represents a pioneering extension of NeRF to semantic radiance fields, which augments rendered outputs with instance segmentation, thereby supporting diverse downstream perception tasks. [9], [120] follows PNF to additionally

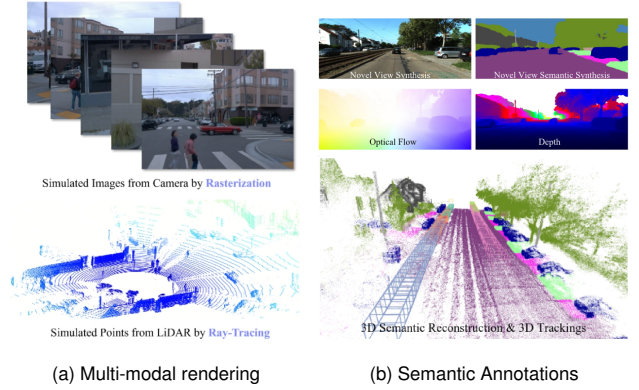


Fig. 7: Visualization of Rendering Modalities. (a): Synchronized image and point cloud rendering from Uni-Gaussians [10]; (b): Comprehensive annotations from HUGS [120], including semantic segmentation for both image and point cloud, optical flow and depth image.

incorporate instance segmentation annotations, and [9], [108], [114]–[116], [120] provide semantic segmentation results.

**Vehicle pose**, which provides positional information of surrounding vehicles, constitutes a critical component in scene understanding, with standard formats including 3D bounding boxes and waypoints. While conventional approaches require pose as explicit input, emerging methods not only eliminate this dependency but also pose during 3D reconstruction. SUDS [9] derives bounding boxes via PCA from instance segmentation results of 3D point cloud, while [101], [116] optimizes parameterized pose within their training frameworks.

**Motion fields**, including 2D optical flow, 3D scene flow and velocity field, reflect the motion patterns of the scene.

**Optical flow** refers to the 2D motion field of pixels between consecutive frames in an image sequence, enhancing spatial-temporal coherence in rendering [20], [107], [108], [120]. [107], [108] introduces optical flow as a cross-view geometric consistency regularization to mitigate aliasing artifacts. HUGS and HUGSIM [20], [120] leverage supervision over optical flow to improve the rendered depth image.

**Scene flow** extends this concept to 3D, describing the 3D motion of objects in the scene. Several approaches [9], [68], [128] leverage scene flow to aggregate temporal information and enforce spatial correspondence in adjacent frames, effectively enhancing the temporal coherence of dynamic agents.

**Velocity field** normalizes the scene flow along the temporal dimension, thereby providing a quantitative ground truth for downstream tasks such as object tracking. The reformulation of 3D Gaussian in PVG [115], [118], [119] inherently incorporates velocity attributes, while EMD [129] learns a deformation field of the scene at each time step, both of them enables direct calculation of velocity fields.

### B. Localization & Mapping

Precise localization and high-fidelity mapping form the foundational spatial intelligence for autonomous vehicles, enabling safe navigation and context-aware decision-making. 3D

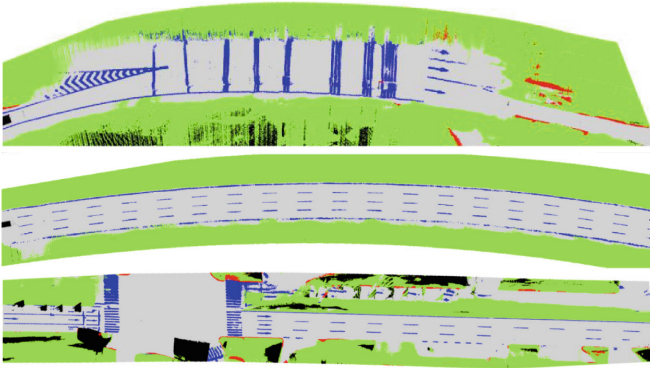


Fig. 8: Semantic map from EMIE-MAP [14].

reconstruction, particularly through 3DGS, delivers a groundbreaking spatial representation for SLAM systems via real-time photorealistic rendering capabilities, significantly enhancing robustness in complex outdoor environments. [143]–[145] jointly advance online dense mapping through continuous scene representation optimization and achieve centimeter-level localization accuracy via iterative pose refinement. BEV-GS [146] recovers fine-grained road surface details such as road surface materials, markings, and damages, enhancing the smoothness and comfort of motion planning.

Semantic map (Fig. 8) provides a structured representation of the environment, encoding semantic information like lane markings, traffic signs, and road types. Previous semantic map extraction relied on manual annotation, incurring significant labor and financial costs while struggling to maintain map freshness. Road surface reconstruction methods [14], [83], [147]–[149] incorporate semantic information modeling during reconstruction, enabling online extraction of semantic maps. These maps support tasks such as navigation and path planning, while also providing pseudo-ground truth for scene understanding tasks like lane line detection.

### C. Scene Understanding

Rather than advancing reconstruction methodologies, contemporary approaches prioritize novel system integration with 3D reconstruction through optimized architectures and training paradigms, directly boosting the perceptual accuracy and scene comprehension ability of autonomous driving systems.

StreetUnveiler [89] extends static background reconstruction by detecting and filtering out stationary traffic participants (e.g., parked vehicles) to extract unoccluded driving scene infrastructure, thereby providing more stable reference for environmental understanding and HD map generation.

3D reconstruction enhances perception modules of autonomous driving systems by encoding persistent scene knowledge and completing missing geometry [12], [13]. PreSight [12] leverages NeRF to construct static prior memories based on historical observations, which encodes city-scale NeRF reconstructions in memory, enabling efficient environmental context augmentation for online perception systems. UniPAD [13] innovatively integrates 3D reconstruction to address partial observation in driving scenarios, enhancing

scene perception and understanding. It integrates masked autoencoders to complete geometry with partially observed images and point clouds, improving performance on tasks like object detection and semantic segmentation.

GaussianAD [15] presents an end-to-end framework which employs 3D Gaussians as unified scene representations, thereby bridging dense tasks (3D semantic occupancy) and sparse tasks (detection/motion prediction). It introduces Gaussian Flow, a 3D Gaussian motion field jointly predicted via neural scene representations and ego-motion trajectory estimation, to enable efficient future scene computation through affine transforms for robust spatial-temporal forecasting.

RAD [11] introduces a simulator-in-loop reinforcement learning framework integrating 3D reconstruction-based simulation for iterative policy optimization. A 3DGS simulator dynamically reconstructs high-risk scenarios through log-replay of traffic participants, enabling adversarial training via edge case generation. The planner is optimized via simulator-derived rewards, achieving progressive performance gains through interaction with cyclical environment.

### D. Simulation

Simulators employ modular architectures and user-friendly interfaces to encapsulate driving scene reconstruction methods, delivering both high-fidelity multimodal sensor simulation and parameterized traffic agent control via scene graphs for open-loop [18] or closed-loop [16], [17], [19], [20] verification.

MARS [18] provides a highly configurable open-loop simulator platform that supports switching between diverse NeRF variants for the backend renderer, multiple ray sampling strategies, and multimodal inputs, yet it only supports simulating scene variations through recorded playback. The open-loop simulation mode fails to provide counterfactual or long-term simulation, significantly limiting its effectiveness in training autonomous driving systems.

Close-loop simulators [16], [17], [19]–[21] enable traffic participants to react to environmental changes, thereby better approximating real-world traffic dynamics and substantially expanding their application scope. To model diverse traffic participants in driving scenarios, UniSim [16] employs a hypernetwork to dynamically generate their features, whereas OASim [17] predefines an asset library of agents. However, these simulators are naturally constrained by the complexity of NeRF, which limits their ability to support real-time rendering.

HUGSIM [20] extends HUGS as a closed-loop simulator, establishing the first 3DGS-based simulator. It outperforms NeRF-based methods in terms of real-time rendering while supporting a diverse range of rendering modalities. HUGSIM integrates a trajectory generator to eliminate manual vehicle trajectory design and incorporates a vehicle asset library reconstructed from 3DRealCar [52] to enhance rendering fidelity.

These simulators primarily focus on enhancing perceptual reconstruction quality, leaving agent behavior underexplored. ChatSim [21] integrates a Large Language Model (LLM) to adjust scenes based on text prompts, enabling functionalities such as adding or removing agents, modifying agent behaviors, and separating foreground and background, providing rich simulation capabilities through a user-friendly method.



### E. Scene Generation

3D generative methods are crucial for scalable scenario synthesis in autonomous driving, reducing reliance on resource-intensive data acquisition and mitigating safety risks associated with collecting rare-edge cases (e.g., extreme weather, collision scenarios) essential for addressing long-tail challenges. Guided by high-level semantic conditions, such as BEV maps and text prompts, these approaches efficiently produce diverse driving scenes at minimal cost. As an integral component of methodological paradigm evolution, generative approaches are comparatively analyzed in Table III.

Existing generative approaches [10], [131] both condition on semantic inputs and leverage video generation models to synthesize perceptual details, albeit through distinct technical pathways, pre-generation and post-generation. MagicDrive3D [131] adopts a pre-generation paradigm that first synthesizes visual details in 2D space before 3D reconstruction. The framework initially employs a video diffusion model to generate surrounding-view videos compliant with BEV layouts from the ego's perspective, then elevates 2D video sequences to 3D point clouds through monocular depth estimation and inverse projection, ultimately fusing both modalities for 3D driving scene generation. UniScene [130] pioneers a post-generation paradigm that first generates BEV-aligned semantic occupancy fields before visual details generation. The method innovatively employs 3DGS as semantic carriers rather than visual information carriers, utilizing an occupancy diffusion model to produce semantic 3D Gaussians conforming to BEV inputs. These semantic 3D Gaussians are subsequently rendered into semantic maps, serving as guidance for video diffusion model to synthesize the final driving video.

While both paradigms achieve novel view synthesis from BEV layouts to arbitrary perspectives under various environmental conditions specified by text prompts (Fig. 9), the pre-generation approach consolidates visual detail generation and viewpoint transformation within a single video diffusion model, exacerbating inherent inter-frame inconsistencies. In contrast, post-generation leverages explicit 3D representations to enable consistent multi-view rendering, significantly improving both temporal coherence and cross-view consistency.

## VII. RETROSPECT & PROSPECT

### A. Technical Evolutions

Learning-based 3D reconstruction techniques for autonomous driving have undergone significant advancements across multiple dimensions, including input modality requirements, methodological paradigms, representation schemes, and computational efficiency.

**1) Input Data Requirements** Early learning-based 3D reconstruction in autonomous driving [100], [105] focused solely on photorealism while neglecting geometric accuracy. Subsequent multimodal approaches [9], [102], [111], [115], [143], [145] achieved high-quality geometric reconstruction by incorporating LiDAR point clouds, but incur significantly increased costs. The dependency of LiDAR substantially limited the practicality of 3D reconstruction, thus driving research toward relaxing input data requirements. Unimodal methods

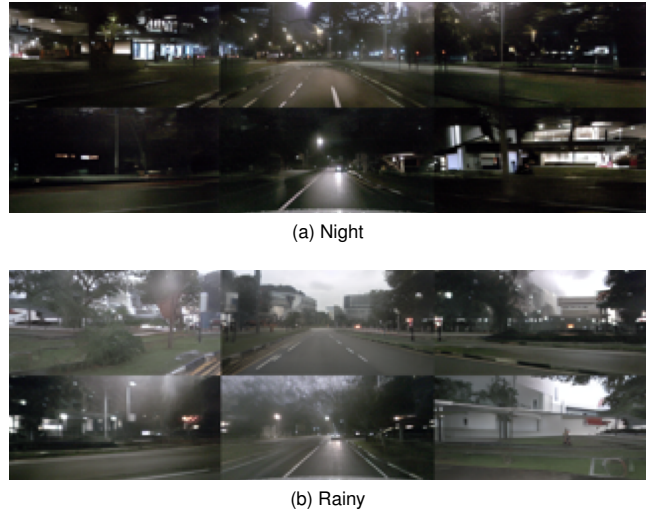


Fig. 9: Synthesized scene under different environmental conditions by UniScene [10].

first eliminated dependence on LiDAR point clouds [110], [113], and some approaches [119], [125], [144] further enabled 3D reconstruction with pose-free visual inputs. Emerging techniques like VGGT [150] have exhibited potential for pose-free 3D reconstruction of driving scenes in feedforward manner.

**2) Methodology Paradigm** The methodological paradigm has evolved from the earliest per-scene optimization [68], [100], [101] to feedforward reconstruction [44], [125], and further to generation [130], [131], significantly streamlining the data acquisition process. Per-scene optimization requires substantial computational resources to reconstruct a scene offline, which fails to meet the data volume demands of contemporary data-driven models and thus lacking practicality. In contrast, feedforward models establish a universal 2D-to-3D mapping to predict scene representations in real-time online, significantly enhancing the scalability of 3D reconstruction methods. Generative models further revolutionize this paradigm by enabling the direct generation of 3D driving scenes from abstract inputs (e.g., text prompts or BEV maps), completely bypassing traditional sensor data acquisition pipelines while maintaining reconstruction quality, propelling data scalability to the next level. This methodological paradigm evolution reflects the field's progression toward efficient, large-scale 3D content creation for autonomous systems.

**3) Representation Evolutions** Representation fundamentally determines the fidelity of driving scene reconstruction, with different representations exhibiting complementary strengths across visual and geometric perspectives. Contemporary research advances along two parallel tracks for fidelity improvement, developing novel 3D representations [100], [102], [109], [117] to improve specific fidelity aspects natively, and creating hybrid representations [81], [83], [84], [88] that combine existing representations to synergize their complementary advantages. Furthermore, 4D representations [9], [68], [115], [124], [127] have been proposed to model the complex spatial-temporal relationships inherent in driving scenarios. The evolution of representations originated from three fundamental



challenges in driving scene reconstruction, visual fidelity, geometric accuracy, and spatial-temporal relationship modeling. While significant progress has been made in rigid object reconstruction, non-rigid agents remain an underexplored frontier.

### B. Challenges & Future Directions

While learning-based 3D reconstruction methods have shown superior capabilities in replicating real-world scenarios and potential in autonomous driving applications, several critical challenges still remain to be addressed in future research.

**1) Close-loop Simulation** Present close-loop simulators mainly focus on reconstruction fidelity yet overlook the behavior distribution of agents in real-world scenarios, with their behavior distributions being either overly simplified [17], [20] or reliant on human intervention [16], [19], [21]. This defect will lead to the overfitting of autonomous driving systems to simple scenarios, compromising their ability to handle real-world complexities. Agent behavior simulation models [151], [152] simulate realistic agent interactions based on historical motion of all agents in the scene and predict future poses, offering authentic scenario evolution. Agent behavior simulation models can be integrated as a plug-and-play module, enabling seamlessly coupling with scene graph-based simulators. End-to-end frameworks that integrate 3D reconstruction with agent behavior simulation may represent the ultimate paradigm for autonomous driving simulation systems.

**2) Weather/Lighting Editing** Autonomous vehicles require robustness in all conditions, but existing datasets and simulators predominantly feature ideal weather and lighting, lacking reflection of adverse weather or low-light scenarios. Weather editing methodologies [153], [154] facilitate the simulation of diverse atmospheric conditions, including rain, snow, and fog, through injecting dynamic particles within scene representations, while driving scene generative models [130], [131] employ video diffusion models to synthesize diverse environmental conditions. While these methods realize a preliminary visual simulation of weather or lighting editing, they are incapable of replicating the optical phenomena arising from environmental changes, such as scattering in foggy conditions or additional reflections generated during rainfall. Physics-based rendering emerges as a promising research direction to address these limitations (e.g., inverse rendering [155]–[160]). Such integration would allow the simulation of complex weather-induced effects with physical realism, such as scattering in fog, or reflections of the road surface on a rainy day. Bridging this gap is crucial for creating all-round simulators to enhancing the robustness of autonomous driving systems under adverse weather and lighting conditions.

**3) Computational Efficiency** Efficiency plays a crucial role in the practicality and scalability of 3D reconstruction methods, primarily determined by their rendering approaches. As seen in Tables II and III, implicit representations like NeRF require dense spatial sampling per view, making real-time rendering impractical, which often requires several seconds to render a single frame even with efficiency-improved variants such as instant-NGP. These methods remain tethered to powerful desktop GPUs. By contrast, explicit representations,

such as neural mesh or 3D Gaussian, leverage rasterization pipelines that deliver real-time performance up to hundreds of FPS, paving the way for mobile readiness.

While many learning-based 3D reconstruction frameworks for autonomous driving achieve efficient reconstruction [87], [116], [121] on a single high-performance GPU, deployment on mobile platform presents distinct challenges. Embedded systems in vehicles are resource-constrained and latency-sensitive. Bridging this gap demands representations and rendering paradigms custom-built for lightweight, heterogeneous hardware. Emerging systems such as SeeLe [161] proposes a renderer which eliminates out-of-view and insignificant Gaussians to save memory and accelerate rendering, while Voyager [162] presents a novel cloud rendering system that only streams newly visible Gaussians to the client based on LoD heuristics with lookup-table rasterization tailored for mobile devices. These mobile-ready pipelines demonstrate that targeted optimizations, such as primitive filtering, cloud-computing system, and view-dependent rendering can unlock real-time, resource-efficient 3D reconstruction on mobile platforms. While current methods offer vital proof-of-concept, truly robust deployment will require continued innovation in compact representation and efficient rendering improvement.

**4) Safety Concerns** As 3D reconstruction gains traction in autonomous driving through data augmentation and closed-loop simulation frameworks, it brings both promising advantages and critical safety concerns. Present 3D reconstruction inevitably introduces perceptual artifacts like edge blurring, aliasing, and semantically inconsistent textures, which can inadvertently undermine downstream perception systems. Meanwhile, simulators [18]–[20] with over-simplified participant behaviors can induce overfitting to easy scenarios, consequently diminishing their robustness to handle complex situations. These technical risks intersect with broader concerns around algorithmic bias: generative and reconstruction pipelines trained on unbalanced data may misrepresent rare scenarios, introducing real-world safety and ethical vulnerabilities. Given these potential risks, the integration of 3D reconstruction technology in safety-critical autonomous driving applications necessitates thorough and systematic validation, particularly field testing with physical vehicles, to maximize its utility while minimizing potential ethical and safety risks. These safety concerns also call for the research community to establish rigorous safety protocols to ensure the fundamental safety standards of autonomous driving systems.

### REFERENCES

- [1] B. Mildenhall, P. P. Srinivasan, M. Tancik, J. T. Barron, R. Ramamoorthi, and R. Ng, “Nerf: Representing scenes as neural radiance fields for view synthesis,” *Communications of the ACM*, vol. 65, no. 1, pp. 99–106, 2021.
- [2] T. Müller, A. Evans, C. Schied, and A. Keller, “Instant neural graphics primitives with a multiresolution hash encoding,” *ACM Transactions on Graphics (TOG)*, vol. 41, pp. 1 – 15, 2022.
- [3] J. T. Barron, B. Mildenhall, M. Tancik, P. Hedman, R. Martin-Brualla, and P. P. Srinivasan, “Mip-nerf: A multiscale representation for anti-aliasing neural radiance fields,” *2021 IEEE/CVF International Conference on Computer Vision (ICCV)*, pp. 5835–5844, 2021.

- [4] J. T. Barron, B. Mildenhall, D. Verbin, P. P. Srinivasan, and P. Hedman, "Mip-nerf 360: Unbounded anti-aliased neural radiance fields," *2022 IEEE/CVF Conference on Computer Vision and Pattern Recognition (CVPR)*, pp. 5460–5469, 2021.
- [5] W. Feng, J. Li, H. Cai, X. Luo, and J. Zhang, "Neural points: Point cloud representation with neural fields for arbitrary upsampling," in *Proceedings of the IEEE/CVF conference on computer vision and pattern recognition*, 2022, pp. 18 633–18 642.
- [6] Q. Xu, Z. Xu, J. Philip, S. Bi, Z. Shu, K. Sunkavalli, and U. Neumann, "Point-nerf: Point-based neural radiance fields," in *Proceedings of the IEEE/CVF conference on computer vision and pattern recognition*, 2022, pp. 5438–5448.
- [7] B. Yang, C. Bao, J. Zeng, H. Bao, Y. Zhang, Z. Cui, and G. Zhang, "Neumesh: Learning disentangled neural mesh-based implicit field for geometry and texture editing," in *European Conference on Computer Vision*. Springer, 2022, pp. 597–614.
- [8] B. Kerbl, G. Kopanas, T. Leimkühler, and G. Drettakis, "3d gaussian splatting for real-time radiance field rendering," *ACM Trans. Graph.*, vol. 42, no. 4, pp. 139–1, 2023.
- [9] H. Turki, J. Y. Zhang, F. Ferroni, and D. Ramanan, "Suds: Scalable urban dynamic scenes," in *Proceedings of the IEEE/CVF Conference on Computer Vision and Pattern Recognition*, 2023, pp. 12 375–12 385.
- [10] Z. Yuan, Y. Pu, H. Luo, F. Lang, C. Chi, T. Li, Y. Shen, H. Sun, B. Wang, and X. Yang, "Uni-gaussians: Unifying camera and lidar simulation with gaussians for dynamic driving scenarios," *arXiv preprint arXiv:2503.08317*, 2025.
- [11] H. Gao, S. Chen, B. Jiang, B. Liao, Y. Shi, X. Guo, Y. Pu, H. Yin, X. Li, X. Zhang *et al.*, "Rad: Training an end-to-end driving policy via large-scale 3dgs-based reinforcement learning," *arXiv preprint arXiv:2502.13144*, 2025.
- [12] T. Yuan, Y. Mao, J. Yang, Y. Liu, Y. Wang, and H. Zhao, "Presight: Enhancing autonomous vehicle perception with city-scale nerf priors," in *European Conference on Computer Vision*. Springer, 2024, pp. 323–339.
- [13] H. Yang, S. Zhang, D. Huang, X. Wu, H. Zhu, T. He, S. Tang, H. Zhao, Q. Qiu, B. Lin *et al.*, "Unipad: A universal pre-training paradigm for autonomous driving," in *Proceedings of the IEEE/CVF Conference on Computer Vision and Pattern Recognition*, 2024, pp. 15 238–15 250.
- [14] W. Wu, Q. Wang, G. Wang, J. Wang, T. Zhao, Y. Liu, D. Gao, Z. Liu, and H. Wang, "Emie-map: Large-scale road surface reconstruction based on explicit mesh and implicit encoding," in *European Conference on Computer Vision*. Springer, 2024, pp. 370–386.
- [15] W. Zheng, J. Wu, Y. Zheng, S. Zuo, Z. Xie, L. Yang, Y. Pan, Z. Hao, P. Jia, X. Lang *et al.*, "Gaussianad: Gaussian-centric end-to-end autonomous driving," *arXiv preprint arXiv:2412.10371*, 2024.
- [16] Z. Yang, Y. Chen, J. Wang, S. Manivasagam, W.-C. Ma, A. J. Yang, and R. Urtasun, "Unisim: A neural closed-loop sensor simulator," in *Proceedings of the IEEE/CVF Conference on Computer Vision and Pattern Recognition*, 2023, pp. 1389–1399.
- [17] G. Yan, J. Pi, J. Guo, Z. Luo, M. Dou, N. Deng, Q. Huang, D. Fu, L. Wen, P. Cai *et al.*, "Oasim: An open and adaptive simulator based on neural rendering for autonomous driving," *arXiv preprint arXiv:2402.03830*, 2024.
- [18] Z. Wu, T. Liu, L. Luo, Z. Zhong, J. Chen, H. Xiao, C. Hou, H. Lou, Y. Chen, R. Yang *et al.*, "Mars: An instance-aware, modular and realistic simulator for autonomous driving," in *CAAI International Conference on Artificial Intelligence*. Springer, 2023, pp. 3–15.
- [19] W. Ljungbergh, A. Tonderski, J. Johnander, H. Caesar, K. Åström, M. Felsberg, and C. Petersson, "Neuroncap: Photorealistic closed-loop safety testing for autonomous driving," in *European Conference on Computer Vision*. Springer, 2024, pp. 161–177.
- [20] H. Zhou, L. Lin, J. Wang, Y. Lu, D. Bai, B. Liu, Y. Wang, A. Geiger, and Y. Liao, "Hugsim: A real-time, photo-realistic and closed-loop simulator for autonomous driving," *arXiv preprint arXiv:2412.01718*, 2024.
- [21] Y. Wei, Z. Wang, Y. Lu, C. Xu, C. Liu, H. Zhao, S. Chen, and Y. Wang, "Editable scene simulation for autonomous driving via collaborative llm-agents," in *Proceedings of the IEEE/CVF Conference on Computer Vision and Pattern Recognition*, 2024, pp. 15 077–15 087.
- [22] L. He, L. Li, W. Sun, Z. Han, Y. Liu, S. Zheng, J. Wang, and K. Li, "Neural radiance field in autonomous driving: A survey," *arXiv preprint arXiv:2404.13816*, 2024.
- [23] Y. Bao, T. Ding, J. Huo, Y. Liu, Y. Li, W. Li, Y. Gao, and J. Luo, "3d gaussian splatting: Survey, technologies, challenges, and opportunities," *IEEE Transactions on Circuits and Systems for Video Technology*, 2025.
- [24] H. Zhu, Z. Zhang, J. Zhao, H. Duan, Y. Ding, X. Xiao, and J. Yuan, "Scene reconstruction techniques for autonomous driving: a review of 3d gaussian splatting," *Artificial Intelligence Review*, vol. 58, no. 1, p. 30, 2024.
- [25] A. Arnal and J. Monterde, "Bézier-smart surfaces of arbitrary degree," *Journal of Computational and Applied Mathematics*, vol. 457, p. 116253, 2025.
- [26] Y.-X. Hao and W.-Q. Fei, "Construction of bézier surfaces with minimal quadratic energy for given diagonal curves," *Journal of Computational and Applied Mathematics*, vol. 446, p. 115854, 2024.
- [27] S. N. I. Rosli and M. I. E. Zulkifly, "Neutrosophic bicubic bezier surface approximation model for uncertainty data," *MATEMATIKA*, vol. 39, no. 3, p. 281–291, Dec. 2023.
- [28] X. Zou, S. B. Lo, R. Sevilla, O. Hassan, and K. Morgan, "The generation of 3d surface meshes for nurbs-enhanced fem," *Computer-Aided Design*, vol. 168, p. 103653, 2024.
- [29] N. Grillanda, A. Chiozzi, G. Milani, and A. Tralli, "Nurbs solid modeling for the three-dimensional limit analysis of curved rigid block structures," *Computer Methods in Applied Mechanics and Engineering*, vol. 399, p. 115304, 2022.
- [30] P. Liu, Y. Zhang, H. Wang, M. K. Yip, E. S. Liu, and X. Jin, "Real-time collision detection between general sdfs," *Computer Aided Geometric Design*, 2024.
- [31] M. Macklin, K. Erleben, M. Müller, N. Chentanez, S. Jeschke, and Z. Corse, "Local optimization for robust signed distance field collision," *Proc. ACM Comput. Graph. Interact. Tech.*, 2020.
- [32] X. Zhu, Y. Xin, S. Li, H. Liu, C. Xia, and B. Liang, "Efficient collision detection framework for enhancing collision-free robot motion," *arXiv preprint arXiv:2409.14955*, 2024.
- [33] M. Yu, T. Lu, L. Xu, L. Jiang, Y. Xiangli, and B. Dai, "Gsdf: 3dgs meets sdf for improved neural rendering and reconstruction," *Advances in Neural Information Processing Systems*, vol. 37, pp. 129 507–129 530, 2024.
- [34] X. Zheng, Y. Liu, P. Wang, and X. Tong, "Sdf-stylegan: implicit sdf-based stylegan for 3d shape generation," in *Computer Graphics Forum*, vol. 41, no. 5. Wiley Online Library, 2022, pp. 52–63.
- [35] M. Li, Y. Duan, J. Zhou, and J. Lu, "Diffusion-sdf: Text-to-shape via voxelized diffusion," in *Proceedings of the IEEE/CVF conference on computer vision and pattern recognition*, 2023, pp. 12 642–12 651.
- [36] K. Zhang, G. Riegler, N. Snavely, and V. Koltun, "Nerf++: Analyzing and improving neural radiance fields," *arXiv preprint arXiv:2010.07492*, 2020.
- [37] Wikipedia contributors, "Bézier surface — Wikipedia, the free encyclopedia," [https://en.wikipedia.org/w/index.php?title=B%C3%A9zier\\_surface&oldid=1197924651](https://en.wikipedia.org/w/index.php?title=B%C3%A9zier_surface&oldid=1197924651), 2024, [Online; accessed 21-March-2025].
- [38] Z. Li, C. Wu, L. Zhang, and J. Zhu, "Dgnr: Density-guided neural point rendering of large driving scenes," *IEEE Transactions on Automation Science and Engineering*, 2024.
- [39] Y. Zhang, Z. Zhu, and D. Du, "Occformer: Dual-path transformer for vision-based 3d semantic occupancy prediction," in *Proceedings of the IEEE/CVF International Conference on Computer Vision*, 2023, pp. 9433–9443.
- [40] Y. Wang, Y. Chen, X. Liao, L. Fan, and Z. Zhang, "Panoocc: Unified occupancy representation for camera-based 3d panoptic segmentation," in *Proceedings of the IEEE/CVF conference on computer vision and pattern recognition*, 2024, pp. 17 158–17 168.
- [41] P. Tang, Z. Wang, G. Wang, J. Zheng, X. Ren, B. Feng, and C. Ma, "Sparseocc: Rethinking sparse latent representation for vision-based semantic occupancy prediction," in *Proceedings of the IEEE/CVF Conference on Computer Vision and Pattern Recognition*, 2024, pp. 15 035–15 044.
- [42] T. Yang, Y. Qian, W. Yan, C. Wang, and M. Yang, "Adaptiveocc: Adaptive octree-based network for multi-camera 3d semantic occupancy prediction in autonomous driving," *IEEE Transactions on Circuits and Systems for Video Technology*, 2024.
- [43] H. Xiao, W. Kang, H. Liu, Y. Li, and Y. He, "Semantic scene completion via semantic-aware guidance and interactive refinement transformer," *IEEE Transactions on Circuits and Systems for Video Technology*, 2024.
- [44] D. Wei, Z. Li, and P. Liu, "Omni-scene: Omni-gaussian representation for ego-centric sparse-view scene reconstruction," *arXiv preprint arXiv:2412.06273*, 2024.
- [45] C. Zhang, H. Song, Y. Wei, C. Yu, J. Lu, and Y. Tang, "Geolrm: Geometry-aware large reconstruction model for high-quality 3d gaussian generation," *Advances in Neural Information Processing Systems*, vol. 37, pp. 55 761–55 784, 2024.

- [46] T. Lu, M. Yu, L. Xu, Y. Xiangli, L. Wang, D. Lin, and B. Dai, "Scaffold-gs: Structured 3d gaussians for view-adaptive rendering," in *Proceedings of the IEEE/CVF Conference on Computer Vision and Pattern Recognition*, 2024, pp. 20 654–20 664.
- [47] Z. Yu, A. Chen, B. Huang, T. Sattler, and A. Geiger, "Mip-splatting: Alias-free 3d gaussian splatting," in *Proceedings of the IEEE/CVF conference on computer vision and pattern recognition*, 2024, pp. 19 447–19 456.
- [48] S. Szymanowicz, C. Rupprecht, and A. Vedaldi, "Splatter image: Ultra-fast single-view 3d reconstruction," *2024 IEEE/CVF Conference on Computer Vision and Pattern Recognition (CVPR)*, pp. 10 208–10 217, 2023.
- [49] J. Zhang, G. Yang, S. Tulsiani, and D. Ramanan, "Ners: Neural reflectance surfaces for sparse-view 3d reconstruction in the wild," *Advances in Neural Information Processing Systems*, vol. 34, pp. 29 835–29 847, 2021.
- [50] T. Liu, H. Zhao, Y. Yu, G. Zhou, and M. Liu, "Car-studio: learning car radiance fields from single-view and unlimited in-the-wild images," *IEEE Robotics and Automation Letters*, vol. 9, no. 3, 2024.
- [51] Z. Yang, S. Manivasagam, Y. Chen, J. Wang, R. Hu, and R. Urtasun, "Reconstructing objects in-the-wild for realistic sensor simulation," in *2023 IEEE International Conference on Robotics and Automation (ICRA)*. IEEE, 2023, pp. 11 661–11 668.
- [52] X. Du, H. Sun, S. Wang, Z. Wu, H. Sheng, J. Ying, M. Lu, T. Zhu, K. Zhan, and X. Yu, "3drealcar: An in-the-wild rgb-d car dataset with 360-degree views," *arXiv preprint arXiv:2406.04875*, 2024.
- [53] C. Ionescu, D. Papava, V. Olaru, and C. Sminchisescu, "Human3.6m: Large scale datasets and predictive methods for 3d human sensing in natural environments," *IEEE Transactions on Pattern Analysis and Machine Intelligence*, vol. 36, no. 7, pp. 1325–1339, jul 2014.
- [54] M. Fieraru, M. Zanfir, S.-C. Pirlea, V. Olaru, and C. Sminchisescu, "Aifit: Automatic 3d human-interpretable feedback models for fitness training," in *The IEEE/CVF Conference on Computer Vision and Pattern Recognition (CVPR)*, June 2021.
- [55] M. Fieraru, M. Zanfir, E. Oneata, A.-I. Popa, V. Olaru, and C. Sminchisescu, "Reconstructing three-dimensional models of interacting humans," *arXiv preprint arXiv:2308.01854*, 2023.
- [56] —, "Learning complex 3d human self-contact," in *Proceedings of the AAAI Conference on Artificial Intelligence*, vol. 35, no. 2, 2021, pp. 1343–1351.
- [57] T. von Marcard, R. Henschel, M. Black, B. Rosenhahn, and G. Pons-Moll, "Recovering accurate 3d human pose in the wild using imus and a moving camera," in *European Conference on Computer Vision (ECCV)*, sep 2018.
- [58] Renderpeople, 2025. [Online]. Available: <https://renderpeople.com/>
- [59] A. Geiger, P. Lenz, and R. Urtasun, "Are we ready for autonomous driving? the kitti vision benchmark suite," in *Conference on Computer Vision and Pattern Recognition (CVPR)*, 2012.
- [60] M. Cordts, M. Omran, S. Ramos, T. Rehfeld, M. Enzweiler, R. Benenson, U. Franke, S. Roth, and B. Schiele, "The cityscapes dataset for semantic urban scene understanding," in *Proc. of the IEEE Conference on Computer Vision and Pattern Recognition (CVPR)*, 2016.
- [61] F. Yu, H. Chen, X. Wang, W. Xian, Y. Chen, F. Liu, V. Madhavan, and T. Darrell, "Bdd100k: A diverse driving dataset for heterogeneous multitask learning," in *Proceedings of the IEEE/CVF conference on computer vision and pattern recognition*, 2020, pp. 2636–2645.
- [62] J. Behley, M. Garbade, A. Milioto, J. Quenzel, S. Behnke, C. Stachniss, and J. Gall, "SemanticKITTI: A Dataset for Semantic Scene Understanding of LiDAR Sequences," in *Proc. of the IEEE/CVF International Conf. on Computer Vision (ICCV)*, 2019.
- [63] H. Caesar, V. Bankiti, A. H. Lang, S. Vora, V. E. Liong, Q. Xu, A. Krishnan, Y. Pan, G. Baldan, and O. Beijbom, "nusenes: A multimodal dataset for autonomous driving," *arXiv preprint arXiv:1903.11027*, 2019.
- [64] P. Sun, H. Kretschmar, X. Dotiwalla, A. Chouard, V. Patnaik, P. Tsui, J. Guo, Y. Zhou, Y. Chai, B. Caine *et al.*, "Scalability in perception for autonomous driving: Waymo open dataset," in *Proceedings of the IEEE/CVF conference on computer vision and pattern recognition*, 2020, pp. 2446–2454.
- [65] Y. Cabon, N. Murray, and M. Humenberger, "Virtual kitti 2," 2020.
- [66] B. Wilson, W. Qi, T. Agarwal, J. Lambert, J. Singh, S. Khandelwal, B. Pan, R. Kumar, A. Hartnett, J. K. Pontes *et al.*, "Argoverse 2: Next generation datasets for self-driving perception and forecasting," *arXiv preprint arXiv:2301.00493*, 2023.
- [67] Y. Liao, J. Xie, and A. Geiger, "KITTI-360: A novel dataset and benchmarks for urban scene understanding in 2d and 3d," *Pattern Analysis and Machine Intelligence (PAMI)*, 2022.
- [68] J. Yang, B. Ivanovic, O. Litany, X. Weng, S. W. Kim, B. Li, T. Che, D. Xu, S. Fidler, M. Pavone *et al.*, "Emernerf: Emergent spatial-temporal scene decomposition via self-supervision," *arXiv preprint arXiv:2311.02077*, 2023.
- [69] Y. Cabon, N. Murray, and M. Humenberger, "Virtual kitti 2," *arXiv preprint arXiv:2001.10773*, 2020.
- [70] M.-F. Chang, J. Lambert, P. Sangkloy, J. Singh, S. Bak, A. Hartnett, D. Wang, P. Carr, S. Lucey, D. Ramanan *et al.*, "Argoverse: 3d tracking and forecasting with rich maps," in *Proceedings of the IEEE/CVF conference on computer vision and pattern recognition*, 2019, pp. 8748–8757.
- [71] R. Zhang, P. Isola, A. A. Efros, E. Shechtman, and O. Wang, "The unreasonable effectiveness of deep features as a perceptual metric," *2018 IEEE/CVF Conference on Computer Vision and Pattern Recognition*, pp. 586–595, 2018.
- [72] K. Simonyan and A. Zisserman, "Very deep convolutional networks for large-scale image recognition," *arXiv preprint arXiv:1409.1556*, 2014.
- [73] S. T. Barratt and R. Sharma, "A note on the inception score," *ArXiv*, vol. abs/1801.01973, 2018.
- [74] M. Heusel, H. Ramsauer, T. Unterthiner, B. Nessler, and S. Hochreiter, "Gans trained by a two time-scale update rule converge to a local nash equilibrium," in *Neural Information Processing Systems*, 2017.
- [75] T. Unterthiner, S. Van Steenkiste, K. Kurach, R. Marinier, M. Michalski, and S. Gelly, "Fvd: A new metric for video generation," 2019.
- [76] A. Gretton, K. M. Borgwardt, M. J. Rasch, B. Schölkopf, and A. Smola, "A kernel two-sample test," *The Journal of Machine Learning Research*, vol. 13, no. 1, pp. 723–773, 2012.
- [77] J. Guo, N. Deng, X. Li, Y. Bai, B. Shi, C. Wang, C. Ding, D. Wang, and Y. Li, "Streetsurf: Extending multi-view implicit surface reconstruction to street views," *arXiv preprint arXiv:2306.04988*, 2023.
- [78] F. Wang, A. Louys, N. Piasco, M. Bennehar, L. Roldão, and D. Tsishkou, "Planerf: Svd unsupervised 3d plane regularization for nerf large-scale scene reconstruction," *arXiv preprint arXiv:2305.16914*, 2023.
- [79] T. Tao, G. Wang, Y. Lao, P. Chen, J. Liu, L. Lin, K. Yu, and X. Liang, "Alignmif: Geometry-aligned multimodal implicit field for lidar-camera joint synthesis," in *Proceedings of the IEEE/CVF Conference on Computer Vision and Pattern Recognition*, 2024, pp. 21 230–21 240.
- [80] X. Weng, Y. Man, J. Park, Y. Yuan, M. O'Toole, and K. M. Kitani, "All-in-one drive: A comprehensive perception dataset with high-density long-range point clouds," 2021.
- [81] J. Ost, I. Laradji, A. Newell, Y. Bahat, and F. Heide, "Neural point light fields," in *Proceedings of the IEEE/CVF Conference on Computer Vision and Pattern Recognition*, 2022, pp. 18 419–18 429.
- [82] F. Lu, Y. Xu, G. Chen, H. Li, K.-Y. Lin, and C. Jiang, "Urban radiance field representation with deformable neural mesh primitives," in *Proceedings of the IEEE/CVF International Conference on Computer Vision*, 2023, pp. 465–476.
- [83] R. Mei, W. Sui, J. Zhang, X. Qin, G. Wang, T. Peng, T. Chen, and C. Yang, "Rome: Towards large scale road surface reconstruction via mesh representation," *IEEE Transactions on Intelligent Vehicles*, 2024.
- [84] X. Shi, L. Chen, P. Wei, X. Wu, T. Jiang, Y. Luo, and L. Xie, "Dhgs: Decoupled hybrid gaussian splatting for driving scene," *arXiv preprint arXiv:2407.16600*, 2024.
- [85] X. Cui, W. Ye, Y. Wang, G. Zhang, W. Zhou, and H. Li, "Streetsurfgs: Scalable urban street surface reconstruction with planar-based gaussian splatting," *arXiv preprint arXiv:2410.04354*, 2024.
- [86] P. Wang, Y. Liu, Z. Chen, L. Liu, Z. Liu, T. Komura, C. Theobalt, and W. Wang, "F2-nerf: Fast neural radiance field training with free camera trajectories," in *Proceedings of the IEEE/CVF Conference on Computer Vision and Pattern Recognition*, 2023, pp. 4150–4159.
- [87] K. Wu, K. Zhang, Z. Zhang, M. Tie, S. Yuan, J. Zhao, Z. Gan, and W. Ding, "Hgs-mapping: Online dense mapping using hybrid gaussian representation in urban scenes," *IEEE Robotics and Automation Letters*, 2024.
- [88] G. Song, C. Cheng, and H. Wang, "Gvxf: Gaussian voxel kernel functions for highly efficient surface reconstruction in open scenes," *Advances in Neural Information Processing Systems*, vol. 37, pp. 104 792–104 815, 2024.
- [89] J. Xu, Y. Wang, Y. Zhao, Y. Fu, and S. Gao, "3d streetunveiler with semantic-aware 2dgs," *arXiv preprint arXiv:2405.18416*, 2024.
- [90] P. Xiao, Z. Shao, S. Hao, Z. Zhang, X. Chai, J. Jiao, Z. Li, J. Wu, K. Sun, K. Jiang *et al.*, "Pandaset: Advanced sensor suite dataset for autonomous driving," in *2021 IEEE international intelligent transportation systems conference (ITSC)*. IEEE, 2021, pp. 3095–3101.

- [91] Z. Feng, W. Wu, T. Deng, and H. Wang, "Rogs: Large scale road surface reconstruction with meshgrid gaussian," 2024. [Online]. Available: <https://arxiv.org/abs/2405.14342>
- [92] J. Wang, S. Manivasagam, Y. Chen, Z. Yang, I. A. Bârsan, A. J. Yang, W.-C. Ma, and R. Urtasun, "Cadsim: Robust and scalable in-the-wild 3d reconstruction for controllable sensor simulation," in *6th Annual Conference on Robot Learning*, 2022.
- [93] P. Wang, L. Liu, Y. Liu, C. Theobalt, T. Komura, and W. Wang, "Neus: Learning neural implicit surfaces by volume rendering for multi-view reconstruction," *ArXiv*, vol. abs/2106.10689, 2021.
- [94] T. Shen, J. Gao, K. Yin, M.-Y. Liu, and S. Fidler, "Deep marching tetrahedra: a hybrid representation for high-resolution 3d shape synthesis," *Advances in Neural Information Processing Systems*, vol. 34, pp. 6087–6101, 2021.
- [95] X. Du, H. Sun, M. Lu, T. Zhu, and X. Yu, "Dreamcar: Leveraging car-specific prior for in-the-wild 3d car reconstruction," *IEEE Robotics and Automation Letters*, 2024.
- [96] Z. Yang, J. Wang, H. Zhang, S. Manivasagam, Y. Chen, and R. Urtasun, "Genassets: Generating in-the-wild 3d assets in latent space," in *Proceedings of the Computer Vision and Pattern Recognition Conference (CVPR)*, June 2025, pp. 22 392–22 403.
- [97] Y. Zhuang, J. Lv, H. Wen, Q. Shuai, A. Zeng, H. Zhu, S. Chen, Y. Yang, X. Cao, and W. Liu, "Idol: Instant photorealistic 3d human creation from a single image," in *Proceedings of the Computer Vision and Pattern Recognition Conference (CVPR)*, June 2025, pp. 26 308–26 319.
- [98] Z. Li, L. Li, and J. Zhu, "Read: Large-scale neural scene rendering for autonomous driving," in *Proceedings of the AAAI Conference on Artificial Intelligence*, vol. 37, no. 2, 2023, pp. 1522–1529.
- [99] A. Ligoeki, A. Jelinek, and L. Zalud, "Brmo urban dataset-the new data for self-driving agents and mapping tasks," in *2020 IEEE International Conference on Robotics and Automation (ICRA)*. IEEE, 2020, pp. 3284–3290.
- [100] J. Ost, F. Mannan, N. Thuerey, J. Knodt, and F. Heide, "Neural scene graphs for dynamic scenes," in *Proceedings of the IEEE/CVF Conference on Computer Vision and Pattern Recognition*, 2021, pp. 2856–2865.
- [101] A. Kundu, K. Genova, X. Yin, A. Fathi, C. Pantofaru, L. J. Guibas, A. Tagliasacchi, F. Dellaert, and T. Funkhouser, "Panoptic neural fields: A semantic object-aware neural scene representation," in *Proceedings of the IEEE/CVF Conference on Computer Vision and Pattern Recognition*, 2022, pp. 12 871–12 881.
- [102] A. Tonderski, C. Lindström, G. Hess, W. Ljungbergh, L. Svensson, and C. Petersson, "Neurad: Neural rendering for autonomous driving," in *Proceedings of the IEEE/CVF Conference on Computer Vision and Pattern Recognition*, 2024, pp. 14 895–14 904.
- [103] M. Alibeigi, W. Ljungbergh, A. Tonderski, G. Hess, A. Lilja, C. Lindström, D. Motornik, J. Fu, J. Widahl, and C. Petersson, "Zenseact open dataset: A large-scale and diverse multimodal dataset for autonomous driving," in *Proceedings of the IEEE/CVF International Conference on Computer Vision*, 2023, pp. 20 178–20 188.
- [104] T. Deng, S. Liu, X. Wang, Y. Liu, D. Wang, and W. Chen, "Prosgnerf: Progressive dynamic neural scene graph with frequency modulated auto-encoder in urban scenes," *arXiv preprint arXiv:2312.09076*, 2023.
- [105] J. Choi, G. Hwang, and S. J. Lee, "Dico-nerf: Difference of cosine similarity for neural rendering of fisheye driving scenes," in *Proceedings of the IEEE/CVF Conference on Computer Vision and Pattern Recognition*, 2024, pp. 7850–7858.
- [106] E. Son, J. Choi, J. Song, Y. Jin, and S. J. Lee, "Monocular depth estimation from a fisheye camera based on knowledge distillation," *Sensors*, vol. 23, no. 24, p. 9866, 2023.
- [107] Z. Xie, J. Zhang, W. Li, F. Zhang, and L. Zhang, "S-nerf: Neural radiance fields for street views," *arXiv preprint arXiv:2303.00749*, 2023.
- [108] Y. Chen, J. Zhang, Z. Xie, W. Li, F. Zhang, J. Lu, and L. Zhang, "S-nerf++: Autonomous driving simulation via neural reconstruction and generation," *IEEE Transactions on Pattern Analysis and Machine Intelligence*, 2025.
- [109] X. Zhou, Z. Lin, X. Shan, Y. Wang, D. Sun, and M.-H. Yang, "Drivinggaussian: Composite gaussian splatting for surrounding dynamic autonomous driving scenes," in *Proceedings of the IEEE/CVF conference on computer vision and pattern recognition*, 2024, pp. 21 634–21 643.
- [110] H. Li, Y. Gao, C. Wu, D. Zhang, Y. Dai, C. Zhao, H. Feng, E. Ding, J. Wang, and J. Han, "Ggrr: Towards pose-free generalizable 3d gaussian splatting in real-time," in *European Conference on Computer Vision*. Springer, 2024, pp. 325–341.
- [111] C. Zhao, S. Sun, R. Wang, Y. Guo, J.-J. Wan, Z. Huang, X. Huang, Y. V. Chen, and L. Ren, "Tclc-gs: Tightly coupled lidar-camera gaussian splatting for autonomous driving: Supplementary materials," in *European Conference on Computer Vision*. Springer, 2024, pp. 91–106.
- [112] Z. Yu, H. Wang, J. Yang, H. Wang, Z. Xie, Y. Cai, J. Cao, Z. Ji, and M. Sun, "Sgd: Street view synthesis with gaussian splatting and diffusion prior," *arXiv preprint arXiv:2403.20079*, 2024.
- [113] Z. Li, Y. Zhang, C. Wu, J. Zhu, and L. Zhang, "Ho-gaussian: Hybrid optimization of 3d gaussian splatting for urban scenes," in *European Conference on Computer Vision*. Springer, 2024, pp. 19–36.
- [114] N. Huang, X. Wei, W. Zheng, P. An, M. Lu, W. Zhan, M. Tomizuka, K. Keutzer, and S. Zhang, "S<sup>3</sup> gaussian: Self-supervised street gaussians for autonomous driving," *arXiv preprint arXiv:2405.20323*, 2024.
- [115] Y. Chen, C. Gu, J. Jiang, X. Zhu, and L. Zhang, "Periodic vibration gaussian: Dynamic urban scene reconstruction and real-time rendering," *arXiv preprint arXiv:2311.18561*, 2023.
- [116] Y. Yan, H. Lin, C. Zhou, W. Wang, H. Sun, K. Zhan, X. Lang, X. Zhou, and S. Peng, "Street gaussians: Modeling dynamic urban scenes with gaussian splatting," in *European Conference on Computer Vision*. Springer, 2024, pp. 156–173.
- [117] Z. Chen, J. Yang, J. Huang, R. de Lutio, J. M. Esturo, B. Ivanovic, O. Litany, Z. Gojcic, S. Fidler, M. Pavone *et al.*, "Omnire: Omni urban scene reconstruction," *arXiv preprint arXiv:2408.16760*, 2024.
- [118] C. Peng, C. Zhang, Y. Wang, C. Xu, Y. Xie, W. Zheng, K. Keutzer, M. Tomizuka, and W. Zhan, "Desire-gs: 4d street gaussians for static-dynamic decomposition and surface reconstruction for urban driving scenes," *arXiv preprint arXiv:2411.11921*, 2024.
- [119] H. Li, J. Li, D. Zhang, C. Wu, J. Shi, C. Zhao, H. Feng, E. Ding, J. Wang, and J. Han, "Vdg: vision-only dynamic gaussian for driving simulation," *arXiv preprint arXiv:2406.18198*, 2024.
- [120] H. Zhou, J. Shao, L. Xu, D. Bai, W. Qiu, B. Liu, Y. Wang, A. Geiger, and Y. Liao, "Hugs: Holistic urban 3d scene understanding via gaussian splatting," in *Proceedings of the IEEE/CVF Conference on Computer Vision and Pattern Recognition*, 2024, pp. 21 336–21 345.
- [121] S. Hwang, M.-J. Kim, T. Kang, J. Kang, and J. Choo, "Vegs: View extrapolation of urban scenes in 3d gaussian splatting using learned priors," in *European Conference on Computer Vision*. Springer, 2024, pp. 1–18.
- [122] M. Khan, H. Fazlali, D. Sharma, T. Cao, D. Bai, Y. Ren, and B. Liu, "Autosplat: Constrained gaussian splatting for autonomous driving scene reconstruction," *arXiv preprint arXiv:2407.02598*, 2024.
- [123] H. Han, K. Zhou, X. Long, Y. Wang, and C. Xiao, "Ggs: Generalizable gaussian splatting for lane switching in autonomous driving," *arXiv preprint arXiv:2409.02382*, 2024.
- [124] G. Zhao, C. Ni, X. Wang, Z. Zhu, X. Zhang, Y. Wang, G. Huang, X. Chen, B. Wang, Y. Zhang *et al.*, "Drivedreamer4d: World models are effective data machines for 4d driving scene representation," *arXiv preprint arXiv:2410.13571*, 2024.
- [125] Q. Tian, X. Tan, Y. Xie, and L. Ma, "Drivingforward: Feed-forward 3d gaussian splatting for driving scene reconstruction from flexible surround-view input," *arXiv preprint arXiv:2409.12753*, 2024.
- [126] G. Hess, C. Lindström, M. Fatemi, C. Petersson, and L. Svensson, "Splatad: Real-time lidar and camera rendering with 3d gaussian splatting for autonomous driving," *arXiv preprint arXiv:2411.16816*, 2024.
- [127] J. Mao, B. Li, B. Ivanovic, Y. Chen, Y. Wang, Y. You, C. Xiao, D. Xu, M. Pavone, and Y. Wang, "Dreamdrive: Generative 4d scene modeling from street view images," *arXiv preprint arXiv:2501.00601*, 2024.
- [128] J. Yang, J. Huang, Y. Chen, Y. Wang, B. Li, Y. You, A. Sharma, M. Igl, P. Karkus, D. Xu *et al.*, "Storm: Spatio-temporal reconstruction model for large-scale outdoor scenes," *arXiv preprint arXiv:2501.00602*, 2024.
- [129] X. Wei, Q. Wuwu, Z. Zhao, Z. Wu, N. Huang, M. Lu, N. Ma, and S. Zhang, "Emd: Explicit motion modeling for high-quality street gaussian splatting," *arXiv preprint arXiv:2411.15582*, 2024.
- [130] B. Li, J. Guo, H. Liu, Y. Zou, Y. Ding, X. Chen, H. Zhu, F. Tan, C. Zhang, T. Wang *et al.*, "Uniscene: Unified occupancy-centric driving scene generation," *arXiv preprint arXiv:2412.05435*, 2024.
- [131] R. Gao, K. Chen, Z. Li, L. Hong, Z. Li, and Q. Xu, "Magicdrive3d: Controllable 3d generation for any-view rendering in street scenes," *arXiv preprint arXiv:2405.14475*, 2024.
- [132] Z. Yang, S. Manivasagam, M. Liang, B. Yang, W.-C. Ma, and R. Urtasun, "Recovering and simulating pedestrians in the wild," in *Proceedings of the 2020 Conference on Robot Learning*, ser. Proceedings of Machine Learning Research, 16–18 Nov 2021, pp. 419–431.
- [133] Z. Yang, S. Wang, S. Manivasagam, Z. Huang, W.-C. Ma, X. Yan, E. Yumer, and R. Urtasun, "S3: Neural shape, skeleton, and skinning



- fields for 3d human modeling,” in *Proceedings of the IEEE/CVF Conference on Computer Vision and Pattern Recognition (CVPR)*, June 2021, pp. 13 284–13 293.
- [134] K. Xie, T. Wang, U. Iqbal, Y. Guo, S. Fidler, and F. Shkurti, “Physics-based human motion estimation and synthesis from videos,” in *Proceedings of the IEEE/CVF International Conference on Computer Vision (ICCV)*, October 2021, pp. 11 532–11 541.
- [135] R. Li, J. Tanke, M. Vo, M. Zollhöfer, J. Gall, A. Kanazawa, and C. Lassner, “Tava: Template-free animatable volumetric actors,” in *European Conference on Computer Vision*. Springer, 2022, pp. 419–436.
- [136] C. Guo, T. Jiang, X. Chen, J. Song, and O. Hilliges, “Vid2avatar: 3d avatar reconstruction from videos in the wild via self-supervised scene decomposition,” in *Proceedings of the IEEE/CVF Conference on Computer Vision and Pattern Recognition*, 2023, pp. 12 858–12 868.
- [137] T. Jiang, X. Chen, J. Song, and O. Hilliges, “Instantavatar: Learning avatars from monocular video in 60 seconds,” in *Proceedings of the IEEE/CVF Conference on Computer Vision and Pattern Recognition*, 2023, pp. 16 922–16 932.
- [138] Z. Qian, S. Wang, M. Mihajlovic, A. Geiger, and S. Tang, “3dgs-avatar: Animatable avatars via deformable 3d gaussian splatting,” in *Proceedings of the IEEE/CVF conference on computer vision and pattern recognition*, 2024, pp. 5020–5030.
- [139] Z. Li, Z. Zheng, L. Wang, and Y. Liu, “Animatable gaussians: Learning pose-dependent gaussian maps for high-fidelity human avatar modeling,” in *Proceedings of the IEEE/CVF conference on computer vision and pattern recognition*, 2024, pp. 19 711–19 722.
- [140] S. Lee, S. Kim, H. Lee, W.-S. Jeong, and J. H. Lee, “Geoavatar: Geometrically-consistent multi-person avatar reconstruction from sparse multi-view videos,” in *Proceedings of the Computer Vision and Pattern Recognition Conference*, 2025, pp. 21 138–21 147.
- [141] Q. Zhu, Z. Wei, Z. Zheng, Y. Zhan, Z. Yao, J. Zhang, K. Wu, and Y. Zheng, “Rphg: Towards robust neural point-based graphics in the wild,” *arXiv preprint arXiv:2405.05663*, 2024.
- [142] A. X. Chang, T. Funkhouser, L. Guibas, P. Hanrahan, Q. Huang, Z. Li, S. Savarese, M. Savva, S. Song, H. Su, J. Xiao, L. Yi, and F. Yu, “ShapeNet: An Information-Rich 3D Model Repository,” Stanford University — Princeton University — Toyota Technological Institute at Chicago, Tech. Rep. arXiv:1512.03012 [cs.GR], 2015.
- [143] R. Xiao, W. Liu, Y. Chen, and L. Hu, “Liv-gs: Lidar-vision integration for 3d gaussian splatting slam in outdoor environments,” *IEEE Robotics and Automation Letters*, 2024.
- [144] Z. Zhou, S. Upreti, S. Nie, and H. Yang, “Gs-gvins: A tightly-integrated gnss-visual-inertial navigation system augmented by 3d gaussian splatting,” 2025. [Online]. Available: <https://arxiv.org/abs/2502.10975>
- [145] Y. Xie, Z. Huang, J. Wu, and J. Ma, “Gs-livm: Real-time photo-realistic lidar-inertial-visual mapping with gaussian splatting,” *arXiv preprint arXiv:2410.17084*, 2024.
- [146] W. Wu, T. Zhao, C. Peng, L. Yang, Y. Wei, Z. Liu, and H. Wang, “Bev-gs: Feed-forward gaussian splatting in bird’s-eye-view for road reconstruction,” 2025. [Online]. Available: <https://arxiv.org/abs/2504.13207>
- [147] J. Zhang, S. Chen, H. Yin, R. Mei, X. Liu, C. Yang, Q. Zhang, and W. Sui, “A vision-centric approach for static map element annotation,” in *2024 IEEE International Conference on Robotics and Automation (ICRA)*. IEEE, 2024, pp. 15 861–15 867.
- [148] R. Wang, S. Zhang, P. Huang, D. Zhang, and H. Chen, “Nero: Neural road surface reconstruction,” 2024. [Online]. Available: <https://arxiv.org/abs/2405.10554>
- [149] S. Chen, J. Zhang, R. Mei, Y. Cai, H. Yin, T. Chen, W. Sui, and C. Yang, “Camav2: A vision-centric approach for static map element annotation,” 2024. [Online]. Available: <https://arxiv.org/abs/2407.21331>
- [150] J. Wang, M. Chen, N. Karaev, A. Vedaldi, C. Rupprecht, and D. Novotny, “Vggt: Visual geometry grounded transformer,” in *Proceedings of the Computer Vision and Pattern Recognition Conference*, 2025, pp. 5294–5306.
- [151] Z. Zhou, H. Haibo, X. Chen, J. Wang, N. Guan, K. Wu, Y.-H. Li, Y.-K. Huang, and C. J. Xue, “Behaviorgpt: Smart agent simulation for autonomous driving with next-patch prediction,” *Advances in Neural Information Processing Systems*, vol. 37, pp. 79 597–79 617, 2024.
- [152] W. Wu, X. Feng, Z. Gao, and Y. Kan, “Smart: Scalable multi-agent real-time motion generation via next-token prediction,” *Advances in Neural Information Processing Systems*, vol. 37, pp. 114 048–114 071, 2024.
- [153] C. Sang, Y. Qian, J. Zhang, C. Wang, and M. Yang, “Weather-magician: Reconstruction and rendering framework for 4d weather synthesis in real time,” *arXiv preprint arXiv:2505.19919*, 2025.
- [154] C. Qian, W. Li, Y. Guo, and G. Markkula, “Weatheredit: Controllable weather editing with 4d gaussian field,” *arXiv preprint arXiv:2505.20471*, 2025.
- [155] S. Bi, Z. Xu, P. Srinivasan, B. Mildenhall, K. Sunkavalli, M. Hašan, Y. Hold-Geoffroy, D. Kriegman, and R. Ramamoorthi, “Neural reflectance fields for appearance acquisition,” *arXiv preprint arXiv:2008.03824*, 2020.
- [156] J. A. Gardner, E. Kashin, B. Egger, and W. A. Smith, “The sky’s the limit: Relightable outdoor scenes via a sky-pixel constrained illumination prior and outside-in visibility,” in *European Conference on Computer Vision*. Springer, 2024, pp. 126–143.
- [157] Z. Liang, Q. Zhang, Y. Feng, Y. Shan, and K. Jia, “GS-IR: 3D Gaussian Splatting for Inverse Rendering,” in *2024 IEEE/CVF Conference on Computer Vision and Pattern Recognition (CVPR)*, 2024.
- [158] J. Kaleta, K. Kania, T. Trzcinski, and M. Kowalski, “Lumigauss: Relightable gaussian splatting in the wild,” 2024. [Online]. Available: <https://arxiv.org/abs/2408.04474>
- [159] H. Chen, Z. Lin, and J. Zhang, “Gi-gs: Global illumination decomposition on gaussian splatting for inverse rendering,” in *ICLR*, 2025.
- [160] L. Zhang, A. Rao, and M. Agrawala, “Scaling in-the-wild training for diffusion-based illumination harmonization and editing by imposing consistent light transport,” in *The Thirteenth International Conference on Learning Representations*, 2025.
- [161] X. Huang, H. Zhu, Z. Liu, W. Lin, X. Liu, Z. He, J. Leng, M. Guo, and Y. Feng, “Seele: A unified acceleration framework for real-time gaussian splatting,” *arXiv preprint arXiv:2503.05168*, 2025.
- [162] Z. Liu, H. Zhu, X. Li, Y. Wang, Y. Shi, W. Li, J. Leng, M. Guo, and Y. Feng, “Voyager: Real-time splatting city-scale 3d gaussians on your phone,” 2025. [Online]. Available: <https://arxiv.org/abs/2506.02774>

## VIII. BIOGRAPHY

**Liewen Liao** received a Master’s degree in Computer Science from Shanghai Jiao Tong University, Shanghai, China, in 2022. He is working towards a Ph.D. degree in Control Science and Engineering from Shanghai Jiao Tong University. His main fields of interest are 3D reconstruction, 3D generation and close-loop simulation in autonomous driving.

**Weihao Yan** received a Bachelor’s degree in Automation from Shanghai Jiao Tong University, Shanghai, China, in 2020. He is working towards a Ph.D. degree in Control Science and Engineering from Shanghai Jiao Tong University. His main fields of interest are autonomous driving systems, computer vision, and domain adaptation. His current research activities include virtual-to-real transfer learning, scene segmentation, and foundation models.

**Wang Xu** Wang Xu received the B.S. in school of instrument science and technology from the Southeast University, Nanjing, China, in 2022. He is currently working toward the Ph.D degree in Control Science and Engineering at Shanghai Jiao Tong University. His research interests main include 3D scene reconstruction, computer vision and autonomous driving simulation.

**Ming Yang** received the Master and Ph.D. degrees from Tsinghua University, Beijing, China, in 1999 and 2003, respectively. He is currently the Full Tenure Professor at Shanghai Jiao Tong University, the deputy director of the Innovation Center of Intelligent Connected Vehicles. He has been working in the field of intelligent vehicles for more than 20 years. He participated in several related research projects, such as the THMR-V project (first intelligent vehicle in China), European CyberCars and CyberMove projects, CyberC3 project, CyberCars-2 project, ITER transfer cask project, AGV, etc.

**Songan Zhang** received B.S. and M.S. degrees in automotive engineering from Tsinghua University in 2013 and 2016, respectively. Then, she went to the University of Michigan, Ann Arbor, and got a Ph.D. in mechanical engineering in 2021. After graduation, she worked at Ford Motor Company in the Robotics Research Team as a research scientist. Presently, she is an assistant professor at the Global Institute of Future Technology (GIFT) in Shanghai Jiao Tong University. Her research interests include accelerated evaluation of autonomous vehicles, model-based reinforcement learning, and meta-reinforcement learning for autonomous vehicle decision-making.